Surface Engineering the Cellular Microenvironment via Patterning and Gradients

Aftin M. Ross,[1,2] Joerg Lahann[1,2,3,4,5]

[1]Institute of Functional Interfaces, Karlsruhe Institute of Technology, Hermann-von-Helmholtz-Platz 1, Eggenstein-Leopoldshafen 76344, Germany

[2]Department of Biomedical Engineering, University of Michigan, Ann Arbor, Michigan 48109

[3]Department of Chemical Engineering, University of Michigan, Ann Arbor, Michigan 48109

[4]Department of Materials Science and Engineering, University of Michigan, Ann Arbor, Michigan 48109

[5]Department of Macromolecular Science and Engineering, University of Michigan, Ann Arbor, Michigan 48109

Correspondence to: J. Lahann (E-mail: lahann@umich.edu)

Received 13 December 2012; revised 25 January 2013; accepted 25 January 2013; published online 1 March 2013
DOI: 10.1002/polb.23275

ABSTRACT: Cell organization, proliferation, and differentiation are impacted by diverse cues present in the cellular microenvironment. As a result, the surface of a material plays an important role in cellular function. Synthetic surfaces may be augmented by physical as well as chemical means. In particular, patterning and interfacial gradients may be utilized to mitigate the cellular response. Patterning is advantageous as it affords control over a range of feature sizes from several nanometers to millimeters. Gradients exist *in vivo*, for instance in stem cell niches, and the ability to create interfacial gradients *in vitro* can provide valuable insights into the influence of a series of minute surface changes on a single sample. This review focuses on fabrication methods for generating micro- and nanoscale surface patterns as well as interfacial gradients, the impact of these surface modifications on the cellular response, and the advantages and challenges of these surfaces in *in vitro* applications. © 2013 Wiley Periodicals, Inc. J. Polym. Sci., Part B: Polym. Phys. **2013**, *51*, 775–794

KEYWORDS: bioengineering; biological applications of polymers; surfaces

INTRODUCTION In addition to cell–cell interactions, a myriad of environmental cues [including physical and chemical properties of the extra cellular matrix (ECM)] signal cellular actions.[1] Understanding the cellular response to these environmental cues has a host of important implications in basic science, medical implants, diagnostics, and therapeutics.[2,3] Patterning and gradient techniques afford control of physical and chemical surface characteristics on the level of cellular action, that is, on the micro- and nanoscale.[4] Feature sizes as small as tens of nanometers are possible with current patterning and/or gradient techniques.[5,6] Importantly, a diversity of cell behaviors ranging from cell orientation, cell motility, surface antigen display, activation of tyrosine kinases, and modulation of intracellular signaling, were found to be associated with geographic changes on the nanoscale.[7] Gradients exist *in vivo* providing directional cues for immune cells to an infection site as a part of an immune response[8] or in development as inducements of cellular differentiation resulting in functional glands such as the mammalian pituitary gland.[9] Generating *in vitro* gradients gives scientists an opportunity to explore distinct surface compositions at the cellular level. Furthermore, the use of surface gradients allows for discrete surface chemistries and morphologies to be assessed on a single sample allowing for more efficient screening of materials. This may prove to be more cost-effective and may enable high throughput evaluation.[10,11]

Currently employed patterning methods include photolithography,[12] soft-lithography,[13] microfluidic patterning,[14] laminar flow patterning,[15] stenciling,[16] and a range of techniques for the fabrication of nano-scaled patterns such as electron beam lithography,[17] dip-pen nanolithography (DPN),[18] imprint lithography,[19] or colloidal lithography.[20] These techniques allow for the attachment of biomolecular factors (e.g., proteins, growth factors, cytokines) by both physical adsorption and covalent immobilization. In addition, a host of methods exist for the generation of interfacial gradients.[21-23] Often chemical gradients, as evidenced by a differential concentration of a given ligand across the surface are employed in the investigation of cellular chemotaxis for numerous healthcare applications.[24,25] Furthermore, physical gradients which vary in elasticity or stiffness as a function of distance,[26] as well as those that differ in terms of surface roughness have been created to examine directional cellular responses.[27] Gradient and pattern generating techniques make use of a breadth of materials (metals,[28] natural[29] and

Aftin Ross earned her PhD in the Department of Biomedical Engineering (BME) at the University of Michigan, Ann Arbor (MI) in 2012 under the tutelage of Joerg Lahann. She was awarded a prestigious Whittaker International Scholars postdoctoral fellowship and is currently pursuing postdoctoral research at the Karlsruhe Institute of Technology in Karlsruhe Germany. Her research interests include the design and surface modification of biomaterials for applications including tissue engineering and biomacromolecular self-assembly.

Joerg Lahann has been promoted early to the ranks of Associate Professor with tenure (2008) and Professor (2012) at the University of Michigan. Prof. Lahann has been appointed as the inaugural Director of the new Biointerfaces Institute at the University of Michigan. Since 2009, he is also co-Director of the Institute for Functional Interfaces at the Karlrsruhe Institute of Technology, Germany. He has been selected by Technology Review as one of the top 100 young and the recipient of the 2007 Nanoscale Science and Engineering Award, a NSF-CAREER award, and both a single-PI and a team Idea award (2006 & 2011) from the US Department of Defense. Since 2011, he has been a fellow of the American Institute of Medical and Biological Engineering. He has contributed to more than 135 publications in a wide spectrum of scientific journals with some of the highest impact factors in the field, including *Science, Nature Materials, Nature Biotechnology, Nature Protocols, Nature Nanotechnology, Analytical Chemistry, Applied Physical Letters, Angewandte Chemie, Journal of the American Chemical Society (JACS), Advanced Materials, Biomaterials, or Proceedings of the National Academy of Sciences (PNAS).* Throughout Lahann s career, translation of basic research findings has been an important aspect and Joerg Lahann has contributed to a total of 18 technology disclosures at the University of Michigan (total number of patents and patent applications: <30), several of which were licensed to companies for further technology development. He is also a co-funder of Cambridge-based Seventh Sense Biosystems.

synthetic polymers,[30] glass,[31] etc.) and have numerous methods of action, such as light or physical masking.

This review will provide an overview of current developments in the evaluation and fabrication of micro- and nano-topological patterns and gradients for cellular studies. Specific consideration will also be given to the phenotypic response of various cell types as a result of cellular interactions to various topological cues. Moreover, the advantages and challenges encountered through the use of these techniques will be highlighted for the study of cell-surface interactions in *in vitro* settings.

PATTERNING

Patterning provides scientists with a diverse toolbox for the study of cells and biomolecules. In fact, patterning has been used extensively in biotechnology in areas such as biosensing, tissue engineering, and drug screening.[32] Patterning techniques can create feature sizes ranging from several nanometers to millimeters (or more) and their sizing difference affects different aspects of cell behavior.[33,34] For example, patterning by microfluidic techniques has achieved directional control over nerve regeneration[35] and cell spreading.[36] Surface patterning using local geometric control can guide cell spreading and shape and was found to govern the growth and death of individual cells irrespective of the type of biomolecule used to mediate cell adhesion.[37] Moreover, nano-scaled topology modulates interfacial forces and influences cytoskeletal formation and the adsorption and conformation of integrin binding proteins on cell membranes. Patterning may occur directly, that is, the attachment of the biomolecule(s) of interest to the substrate via the patterning medium, or indirectly in which a template of the desired pattern is made on the substrate followed by subsequent attachment of the biomolecule(s). Table 1 provides a comparison of selected patterning techniques for biomaterials.

Electron Beam Lithography

Electron beam lithography (EBL) is a top-down patterning approach, which uses direct writing. Originally developed for the semiconductor industry, it has been utilized in biology to create patterns for subsequent biomolecular immobilization of proteins, peptides, growth factors, and cells to investigate a host of biomolecular interactions.[44] EBL consists of focusing an electron beam onto a substrate covered with an electron beam photoresist. If the resist is positive, the portions exposed to the beam become more soluble in the developer solution that is used to further define the pattern and the converse is true if a negative resist is utilized. EBL occurs under high vacuum. The resolution of this technique is determined by the size of the molecules in the resist and the scattering range of the electrons.[45] Higher electron beam energies lead to smaller feature sizes and patterns in the 10 nm range have been fabricated using this method.[46] Though small feature sizes can be created, the adoption of this patterning technique is limited by high costs as compared to other lithographic approaches. In addition, the patterning speed of this technique is relatively slow as compared to photolithography. Nonetheless, the technique has been

TABLE 1 Comparison of the Various Patterning Techniques Employed to Investigate Cell Behavior

Technique	Length Scale (μm)	Advantages	Limitations	Biomolecular Patterning Approach
Electron beam lithography	0.005[38]	High resolution. Compatible with standard microfabrication techniques which allows its incorporation into biochips and biosensors.	Relatively expensive. Slow patterning speed.	Indirect
Photolithography	0.1[39]	Varied patterns over large areas. Compatible with numerous substrates	Relatively expensive. High resolution.	Indirect
Soft lithography	0.1[40]	Simple implementation and patterning of large areas. Relatively inexpensive.	Cannot simultaneously print multiple inks. Concerns with ink diffusion.	Direct
Dip pen nanolithography	0.015[41]	Writing can occur within patterns to create complex surface architectures. Compatible with broad range of inks and can be used for high-throughput applications.	Printing quality dependent on a myriad of environmental and system parameters	Either
Colloidal lithography	0.01[42]	Relatively inexpensive and simple. Rapid and patterns large surface areas. Capable of 3D patterning.	Reduced user-defined control of size and geometries as these dependent on particle physics.	Indirect
Microfluidic patterning	0.1[43]	Relatively inexpensive. Rapid, dynamic systems. Multiple ligands and cells can be patterned and subcellular processes studied.	Channel geometry limits pattern diversity.	Direct

utilized to study cell adhesion,[47] stem cell differentiation,[48] and to control cell growth and organization.[49]

Fueled by recent progress with their expansion and differentiation, there is a great deal of interest in stem cells for regenerative medicine and therapeutics.[50] As such there is a growing need to explore factors that influence stem cell phenotype and controlled differentiation. EBL has been utilized to pattern stem cell substrates. For example, Kantawong et al.[48] employed EBL to generate a disordered nanopit topography to guide the differentiation of osteoblast progenitor cells on a biodegradable polyester, polycaprolactone (PCL). A three-step process of EBL, nickel die fabrication, and hot embossing was used to construct a model surface comprised of 120-nm diameter, 100-nm deep pits, in a 300-nm square arrangement from pit center to pit center with controlled error of ± 50 nm in the x–y-direction. Osteoblast progenitor cells were seeded on the surfaces and differential in gel electrophoresis was utilized to analyze the protein expression of cells grown on the disordered nanopit topographies as compared to smooth surfaces. Moreover, histology was used as a complimentary approach to the proteomic assessment and results from both proteomic and histological analysis show that the surfaces displaying topographic features induced differentiation of the progenitor cells faster than those cultured on smooth, planar substrates.

Recently, Dos Reis et al.[49] probed the interactions and networks of neural cells using patterned surfaces, which were created by EBL. A biodegradable hydrogel, poly(amidoamine), was patterned via EBL. After assessing protein adsorption to ensure that proteins adsorbed only on the patterned areas, neuronal cells were seeded onto the patterned substrates. In this instance, the pattern consisted of 10-μm microwells connected by 1 μm microchannels. Cells were provided with neuronal growth factor (NGF) to induce neurite development. Preferential adhesion of the cells to the patterned microwells and neurite outgrowth into the microchannels resulted in the creation of the intercellular neural network shown in Figure 1. Moreover, the number of neurites is determined by the number of microchannels and single cell behavior could be observed. Patterning hydrogels with EBL allows for the creation of complex patterns that afford single cell analysis and thus has applications for multifunctional microdevices as well as the study of single cell behavior in terms of physiological and pharmacological effects.

Photolithography

Photolithography was initially created for use in the semiconductor industry.[33] Nonetheless, it is a technique that has been frequently exploited in the generation of protein and cell patterns.[51–53] In the photolithography process, patterns are generated, when features on a mask are transmitted to a substrate (usually a polymer) by exposure to light. Typical photomasks are comprised of optically transparent materials (at the wavelength used for patterning) and may be

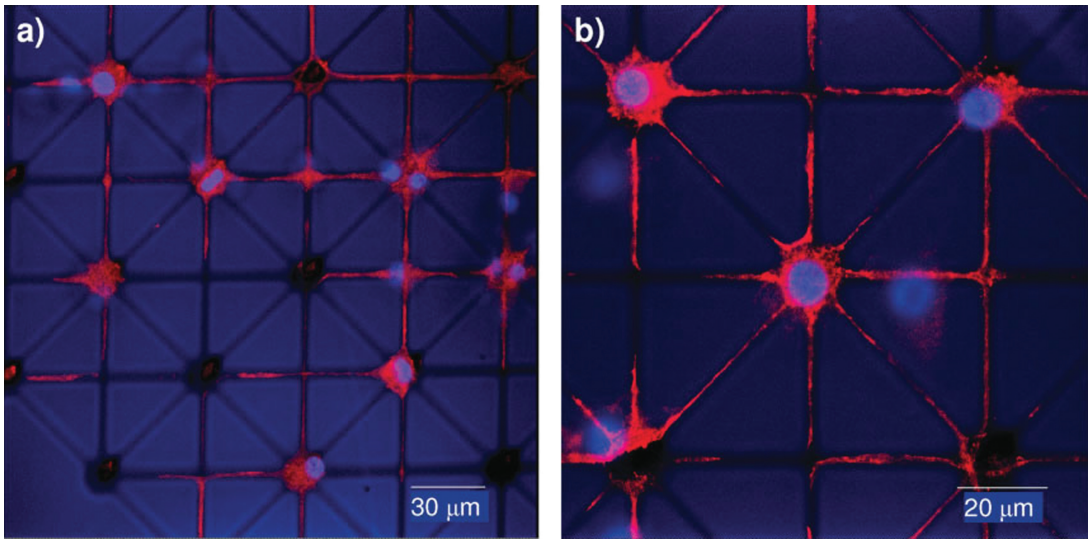

FIGURE 1 Confocal microscopy of neurites grown on EBL patterned microwell networks (10 μm diameter) connected by microchannels (1 μm width). Cells were treated with NGF (for 48 h), and immunostained with DAPI (cell nuclei, blue), FITC anti-vinculin antibody (focal contacts, red), and TRITC phalloidin (actin filaments, red). (a) Cell growth and interconnection between neurites (b) single cell in one microwell and extension of neurites along microchannels.[49]

produced economically using computer-aided design software. Conventional photolithographic processing occurs in a clean room and requires expensive equipment. Thus, the process can be cost prohibitive, if such facilities are not readily accessible. In addition, photolithography is not well suited for patterning on constructs that have previously been functionalized with delicate ligands. Conversely, photolithographic techniques that obviate the need for clean room facilities have emerged such as microscope projection photolithography.[54] Photolithography offers access to feature sizes on the order of 1 μm or less and can be used to create various patterns over large surface areas.[55]

Numerous substrates can be patterned via photolithographic techniques including metal oxides,[56] polymers,[57] glass,[58] and hydrogels.[59] For example, Scotchford et al. fabricated micropatterns of various combinations of metal oxides, titanium (Ti), aluminum (Al), vanadium (V), and niobium (Ni), to investigate protein adsorption and adhesion of human osteoblasts.[60] Surfaces consisted of a background metal oxide and a patterned (stripes or dots) foreground oxide. The first step in creating these surfaces was a vapor deposition process which was used to coat the silicon wafer with a background layer of one of the metal oxides. The second step consisted of spin coating a positive photoresist onto the metal oxide coated wafer, crosslinking of exposed photoresist areas as a result of mercury lamp exposure, and subsequent removal of the crosslinked photoresist via a developer solution. Next, a vapor deposition process of a second metal oxide layer (this layer is different from the background metal oxide and is called the foreground layer) onto exposed areas of the background metal oxide was undertaken. The final step in the pattern generation was the crosslinking of the remaining photoresist and removal of the photoresist via dissolution in developer. This process yielded foreground oxide patterns of stripes or dots 50, 100, and 150 μm in width or diameter in a background oxide layer. Osteoblasts were seeded onto the patterned substrates and cell behavior was observed after 24 h.[60] Numerous materials combinations of the various metal oxides were generated and of these, aluminum was the least biologically favored material irrespective of which oxide it had been combined with. When patterned with other oxides, cells migrated preferentially away from the aluminum and onto the other oxide. This response was attributed to preferential adsorption of cell binding proteins onto the other oxide types, which was validated by subsequent protein adsorption experiments. The results of this work are applicable to studying physical and chemical parameters influencing cell adhesion and migration.

Hahn et al.[59] used transparency-based photolithography to pattern a photoactive poly(ethylene glycol) (PEG)-diacrylate (PEGDA) hydrogels. This method does not require the use of a clean room and is less expensive as transparencies are created using standard ink jet printers. In this instance, the authors investigated the impact of exposure time on the concentration of immobilized biomolecules and the influence of patterning on the adhesion behavior of human dermal fibroblasts (HDFs). The biomolecules, a generic adhesion peptide (RGDS) and an endothelial cell specific adhesion peptide (REDV), were immobilized on the hydrogel by sequential application of the patterning technique. Immobilization occurred by mixing a precursor solution of monoacryloyl-PEG-peptide with a photoinitiator, layering the solution on the hydrogel surface, and then spatio-selectively conjugating the acrylated moieties via UV exposure through a photomask. The concentration of biomolecules on the surface varied linearly with exposure time with increased exposure leading to higher concentrations of immobilized peptides. To ascertain the biological activity of the immobilized peptides, HDFs

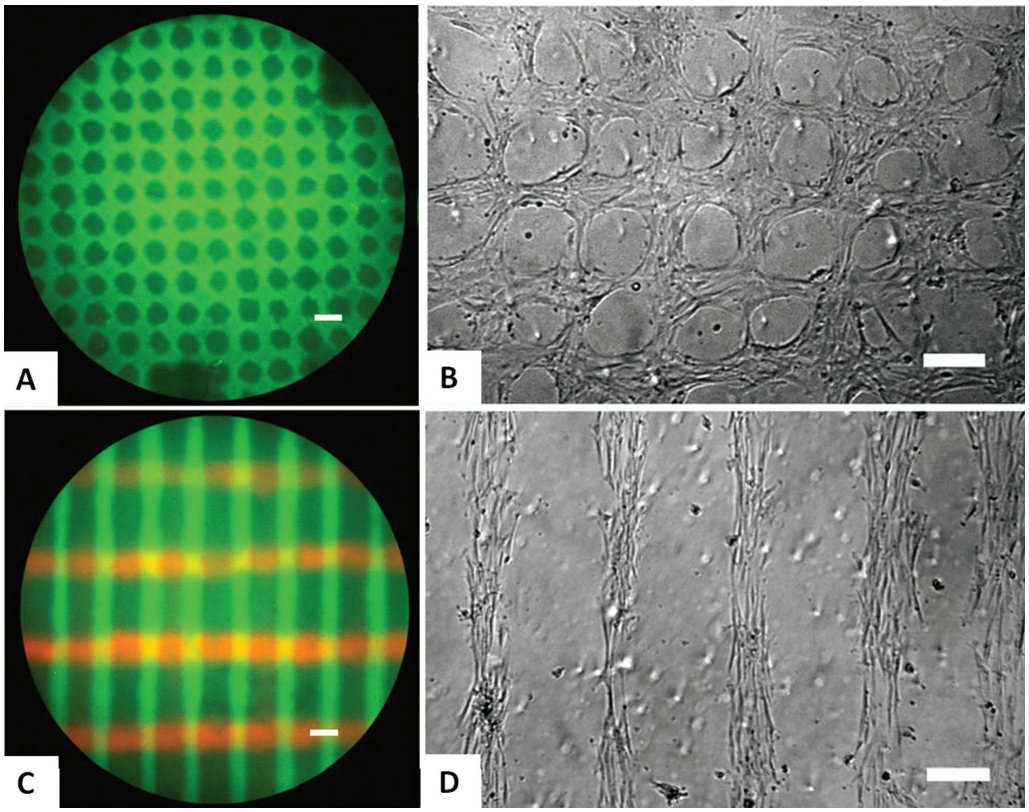

FIGURE 2 Fluorescence of PEGDA hydrogels patterned with (a) ACRL-PEG-RGDS peptide (green). (c) ACRL-PEG-REDV peptide (red) and ACRL-PEG-RGDS peptide (green). Phase contrast of HDFs attached to the surface of the ACRL–PEG–RGDS patterned hydrogels. Note that in (d), HDFs have bound to RGDS patterned regions but not to REDV patterned regions, as expected. (Scale bar = 200 μm).[59]

were seeded onto the patterned surfaces. HDF adhesion was controlled such that cells adhered only to the RGDS patterned regions and not to the REDV areas (Fig. 2).

Microscope projection photolithography uses the fluorescent light from the microscope as the UV irradiation source. Recently, Kim et al.,[61] exploited this technique to pattern multiple proteins and cells. They created a new protein friendly photoresist, poly(2,2-dimethoxy nitrobenzyl methacrylate-r-methyl methacrylate-r-poly(ethylene glycol) methacrylate) (PDMP) that could dissolve upon UV exposure in aqueous environments with a pH $>$ 6.9. PDMP was assessed in terms of its ability to pattern a protein array and its ability to support cellular adhesion of multiple cell types. The PDMP was spin-coated over a biotinylated substrate and then subsequently exposed to UV irradiation, which made the biotin accessible for protein binding. Biotin is known to have a strong affinity for the protein streptavidin (sAV).[62] After the first UV exposure, the patterned surface was incubated with fluorescent sAV. Following rinsing, the microscope was used to align the sample such that new areas of the surface could be irradiated for subsequent protein binding. This process was repeated until an array of three proteins was created. The aforementioned multiple-protein patterning approach was then utilized to create two-component immune cell arrays. Specifically, DO11.10 $CD4^+$ T cell blasts and biotinylated A20 cell lymphomas (A20B) were attached to the cell array. Adherence of the T cell type was facilitated via the use of a biotinylated antibody for this cell type and A20B cells could interact with the surface directly because of its biotin moiety. The T-cell was patterned first followed by the patterning of the A20B cells (Fig. 3). These cells are commonly paired to explore immunological synapses developed among T cells and antigen presenting cells. As such, this platform could serve as a viable option for investigating the intercellular communication between immune cells.

Soft Lithography

Soft lithography takes advantages of printing and molding with elastomeric stamps.[63] The elastomeric stamp is patterned in bas-relief from a replica mold previously created via microfabrication.[64] Transfer of the pattern to the elastomeric stamp is facilitated by the rigidity of the master, which allows for the separation of the master from the mold. Once the elastomeric stamp is created, it is "inked" with a molecule of interest and then brought into physical contact with a substrate. Replica molds, or masters can be patterned with a range of geometries. The feature size is limited by the resolution of the photomask used to create the mold as well as the diffusion of the inks. Patterns as small as tens of nanometers can be created on the molds, [65] however, for biological applications, even feature sizes on the order of 100 nm

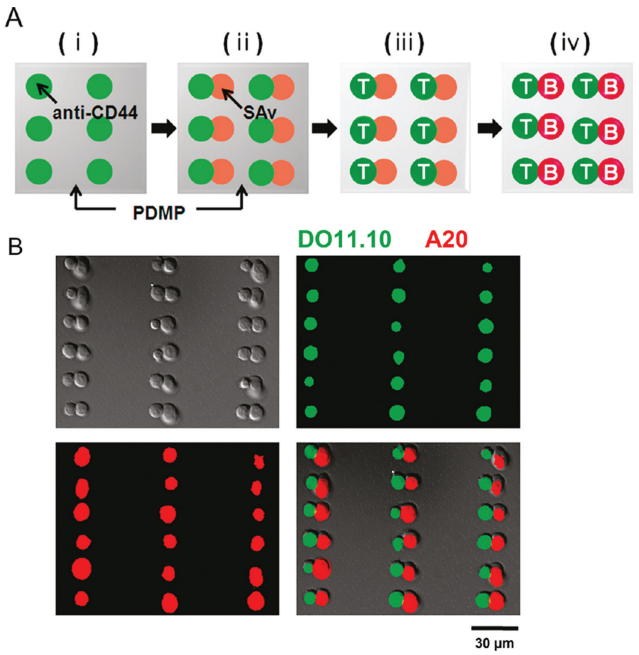

FIGURE 3 Cell array generated via photolithography. (a) Schematic of T/B cell 2-D array fabrication. (b) Representative images of T/B array. DIC (top left), green fluorescence (top right), red fluorescence (bottom left), and DIC/green/red overlay (bottom right).[61]

are challenging to be realized in practice.[66,67] Elastomeric stamps may pattern large areas at once, but the complexity of surface architecture is limited. Microcontact printing (μCP) is a widely used soft lithographic technique and elastomeric stamps are typically comprised of poly(dimethylsiloxane) (PDMS), although other elastomers may be used.[68,69] For example, Schulte et al.[70] used a perfluoropolyether (PFPE)-based elastomer for printing and in this work cell adhesion, morphology, and spreading of primary human fibroblasts was studied. Composite elastomeric materials may also be utilized and a composite of acrloyloxy perfluoropolyether (a-PFPE) and PDMS was exploited by Truong et al.[71] to create generate defined μCP geometries which compared well with those generated by PDMS stamps alone.

Recently, μCP served as a platform for patterning neuronal stem cells (NSC) on poly-lactic-glycolic acid (PLGA) polymer.[72] NSC patterning is potentially beneficial for neural repair and therapy, because it affords control over the spatial distribution and growth of NSCs.[73] However, difficulties in patterning NSCs have limited swift research progress. In this instance, the authors used a PLGA modified with a hydrophobin II protein as the base substrate. Areas of serum were subsequently patterned via μCP and cells adhered to the patterned area while being repelled from the modified PLGA background. Patterning of NSCs can be utilized in the investigation of cell growth, motility, and differentiation in various environments.

Self-assembled monolayers (SAMs) of alkanethiolates are frequently exploited for μCP for biological applications.[74–76] Lehnert et al.[67] assessed the impact of microenvironment geometries on cellular behavior via μCP. In particular, diverse patterns of a hydrophobic alkanethiol, octadecylmercaptan (ODM), were microcontact printed onto gold-coated glass slides. Square patterns ranged in size from 0.3 to 3 μm square and were between 1 and 30 μm apart center-to-center. After printing, ODM patterns were incubated with ECM proteins fibronectin and vitronectin, which adhered to the patterned areas through hydrophobic interactions. A wide variety of cell types were grown on the patterned areas including mouse melanoma cells, β3-integrin-EGFP transfected B16 cells, buffalo rat liver cells, and NIH 3T3 fibroblasts. Results indicated that cells were capable of adhering and spreading on patterned regions as small as 0.1 μm^2 when the center-to-center spacing of the patterned squares is less than 5 μm. In addition, center-center distances of 5–25 μm led cells to spread such that they mimicked the shape of the ECM pattern. However, at center-to-center distances $\geq$30 μm cells were unable to spread, when patterns were $\geq$1 μm^2 (Fig. 4). Findings from this work can be applied to the creation of microenvironments to control cellular behavior and the design of model substrates for studying cell-ligand interactions. It should be noted however, that the use of SAMs comprised of alkanethiolates is limited for long term cellular studies (on the order of days to weeks), because the integrity of the monolayer is comprised over time due to oxidation and then desorption of the SAM from the substrate surface.[77] In summary, the μCP technology is desirable in that it is simple, rapid, inexpensive, and compatible with a wealth of surface and ligand chemistries.

DPN

DPN is similar to EBL in that it is commonly utilized as a direct writing approach. This method uses an atomic force microscopy (AFM) probe inked with a solution that has a chemical affinity for a given surface. Patterns are written on surfaces by bringing the probe in contact with the surface. The inked AFM probe is scanned across the surface in either contact or tapping mode.[78,79] Printing quality and specificity is influenced by humidity, tip geometry, writing speed, contact time between the tip and substrate, and the properties of the ink and substrate.[80] As a result, controlling environmental factors such as temperature and humidity is important and environmental control chambers and glove boxes are often employed to maintain control of these parameters. DPN is advantageous over traditional direct writing techniques such as μCP in that it allows direct writing of different molecules within a nanostructure thereby generating complex surface architectures. In addition, a broad range of inks, from small organic molecules to biomolecules can be printed with this technique including thiols,[81] proteins,[82] and DNA.[83] Because large pin arrays can be created, writing over large surface areas occurs simultaneously thus making DPN a viable option for high throughput applications.[41]

Sekula et al.[84] exploited DPN's ability to pattern multiple biomolecules at once by creating a biomimetic lipid membrane pattern for cell culture studies. Specifically, lipids with two different functional groups, biotin and nitrilotriacetic

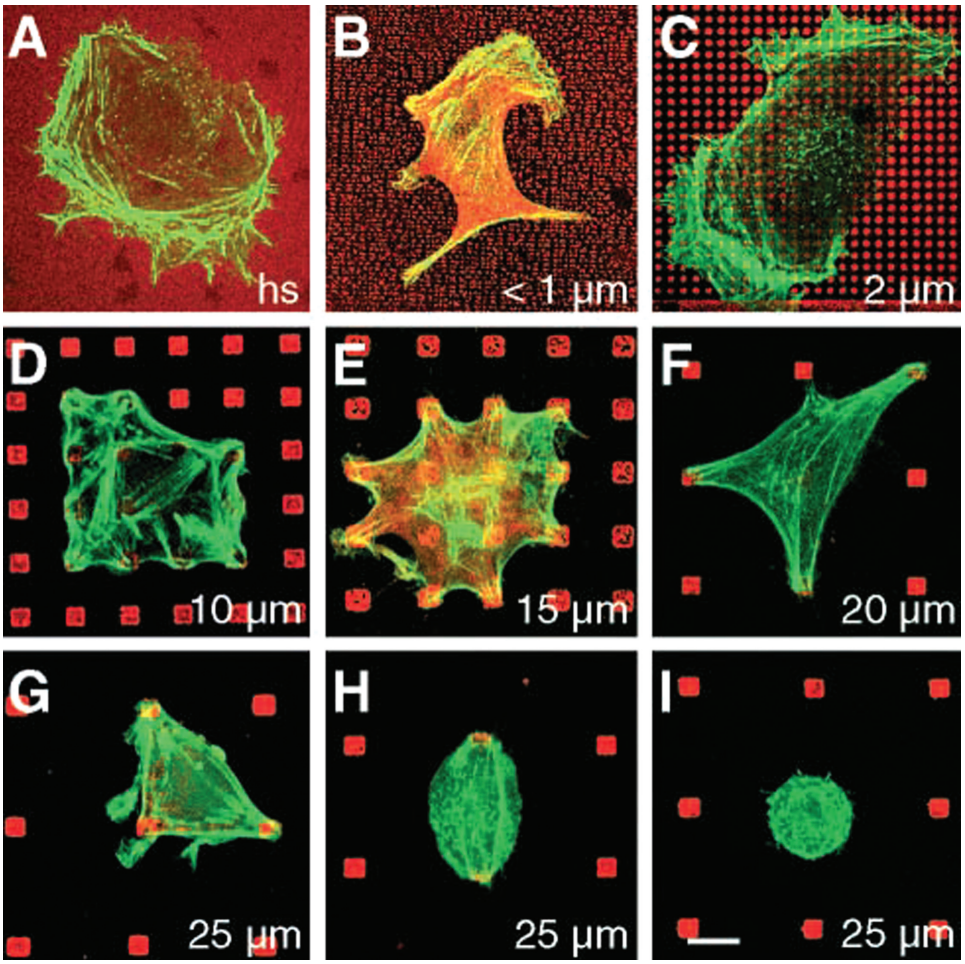

FIGURE 4 Cell spreading as a function of patterning. B16 cells were cultured on fibronectin substrata prepared with μCP and labeled for fibronectin (red) and actin (green). (a) On homogeneous substratum (hs), actin filaments are distributed throughout the cell periphery. (b and c) If the space between dots is 2 μm (b: 0.1 μm^2 squares 1 μm apart, c: 1 μm^2 squares 2 μm apart) cells spread as on a homogeneous substratum. (d–i) Cell growth on patterned substrata of 9 μm^2 dots with spacing as indicated in the right-hand corner. (d–f) With distances of 5-20 μm between dots, cells spread and the actin cytoskeleton formed stress fibers between adjacent dots. (g–i) At 25 μm spacing, spreading was limited and cells became triangular, ellipsoid or round (Scale bar = 10 μm).[67]

acid, were patterned concurrently using a large array. Then selective binding of proteins via sAV-biotin and histidine tag couplings occurred on the patterned areas. The authors verified the functionality of the proteins under numerous environmental conditions. This multilayer protein/lipid pattern, then served as a substrate for T-cell adhesion and activation. T-cells were found to adhere selectively to the curved edges of the patterns and were activated by their interaction with the labeled antibodies in the patterned areas (Fig. 5). The platform provided in this work could be utilized to explore a multitude of biological interactions for applications in diagnostics, drug screenings, and cellular therapies.

Stem cells have also been influenced by the presence of DPN patterns. Curran et al.[85] created DPN arrays of thiols with numerous functionalities on gold. In particular homogenous areas of patterned thiols with end groups (—COOH, —NH_2, —CH_3, —OH) were spaced between 140 nm and 1000 nm apart in order to investigate the relationship between surface chemistry and pitch on mesenchymal stem cell (MSC) behavior. Their work indicated that various combinations of pitch and chemistry can influence the distribution of focal contacts and thus mediate initial cell adhesion. For example, patterned areas with carboxyl groups were found to promote MSC phenotype and adhesion only at a pitch of 280 nm. In addition, variations in pitch were found to impact differentiation of MSCs on OH terminated thiols such that increased pitch, >280 nm, induced differentiation towards an osteogenic lineage. The induced differentiation was attributed to a decrease in cell focal contacts.

Colloidal Lithography

Colloidal lithography is an emerging patterning technique that utilizes two-dimensional (2D) arrays of colloidal particles to generate masks that are utilized in sputtering and etching processes to create patterned features.[86] This technique is advantageous in that it allows for quick surface coverage of large surfaces, is relatively inexpensive, and widely

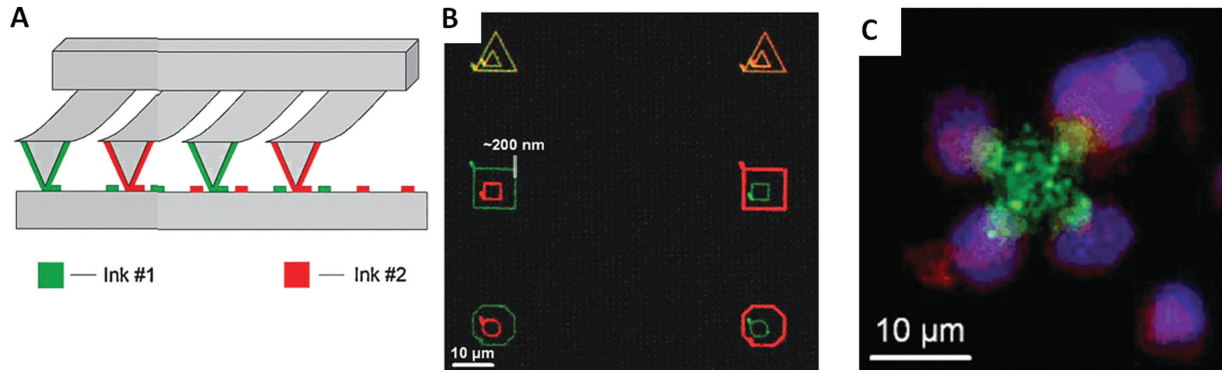

FIGURE 5 Lipid writing via DPN and cellular response to said writing. (a) Schematic of DPN cantilever array used for writing (b) Writing with two fluorophore labeled lipids (rhodamine/red and fluorescein/green). Yellow and orange triangles result from mixing the lipid inks in different concentrations. Fluorescence micrographs of T-cells selectively adhered to and activated by functional proteins bound to phospholipid multilayer patterns via sAV. (c) A three-channel image of T-cells adhering to the corners of lipid protein DPN patterns and activated by functional proteins. Green, red, and blue florescence represent the lipid pattern, cell activation, and Dapi nucleus staining respectively.[84]

available commercially. However, limitations do exist. The particles are self-assembling systems and the size of the features generated is controlled by the size of the particles. Features are also influenced by the particle physics thus making user-defined control of feature size difficult. Without augmentation, patterns generated by particle masks are limited to simple geometries such as triangular and spherical shapes. Particle patterns can be augmented by annealing, reactive ion etching, and ion milling of the particle masks to create more complex/novel geometries.[87,88]

Malmstrom et al.[89] used colloidal lithography to investigate the interaction of breast cancer cells with extracellular matrix (ECM) proteins. In this work, protein patterns of 100, 200, 500, and 1000 nm were created via colloidal lithography to study cell adhesion, spreading, and stress fiber formation on fibronectin patterns. Briefly, physical vapor deposition of titanium and silicon oxide followed by a lift off step transferred the pattern from the colloidal mask to the substrate. The patterned array is then functionalized such that fibronectin is contained in the patterned areas and the background is rendered non-reactive by a poly-L-lysine-g-polyethylene glycol. Results indicated that the size of the protein patches influenced cell adhesion and spreading such that adhesion and spreading increased as pattern size increased (Fig. 6). This work may benefit ECM organization studies and surface signaling investigations for cell culture and tissue engineering applications.

Focal adhesions were also studied by Walter et al., using a colloidal patterning approach.[90] In this work, the authors investigated the force required to remove fibroblasts from

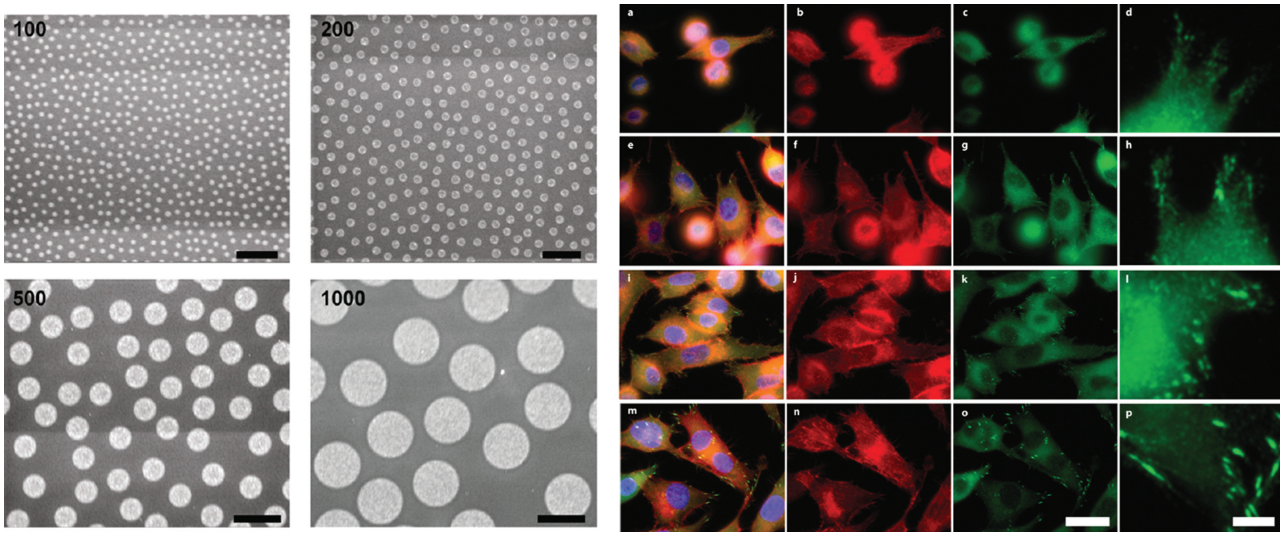

FIGURE 6 SEM images of 100–1000 nm gold holes (bright) in SiO2 film (left). Fluorescence microscopy of breast cancer cells with red staining of actin, green staining of vinculin, and blue DAPI staining of the nucleus on patterned substrates of (a–c) 200 nm (e–g) 500 nm (i–k) 1000 nm (m–o) homogenous control (right) (Scale bar = 30 μm.)[89]

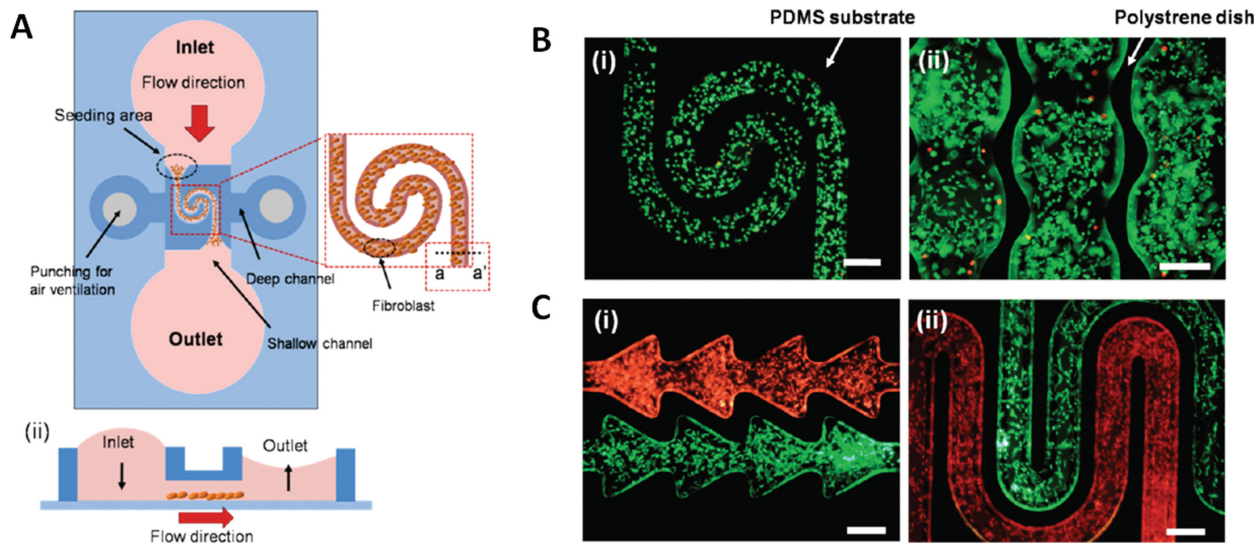

FIGURE 7 Patterned cell culture of fibroblasts or HeLa cells on PDMS coated glass slide controlled via the flooding of channel banks. (a) (i) Schematic illustration of patterned cell culture and (ii) cross sectional view of medium flow. Single and multi-population cell patterning fluorescence images. (b) Spiral patterning on PDMS coated glass slide and (ii) a winding patterning on polystyrene dish. Live cells emit green fluorescence and dead cells emit red fluorescence. (c) (i and ii) Various shaped two population patterning on a polystyrene dish. Red and green cells indicate fibroblast and HeLa cells, respectively (Scale bar = 200 μm.)[94]

colloidal patterned arrays of an integrin binding sequence for ECM proteins, arginine-glysine-aspartic acid (RGD). Magnetic tweezers applied forces of 6–200 pN in the vertical direction to adhered cells on 6 nm ligand patterns distanced 58–145 nm apart. The force required for cellular unbinding from the ligand patterns was negatively correlated to pattern distance with greater release forces being required for smaller pattern distances. Time was also found to play a role, with longer adhesion times requiring greater removal forces. Greater force responses for smaller distances were attributed to increased ligand density on the substrate resulting in better focal adhesions. This approach could be utilized in exploring cellular-biomolecular affinities and the influence of various surface factors on cellular adhesion. In addition to cell adhesion and spreading, colloidal particles have also been utilized to investigate stem cell differentiation.[91]

Microfluidic Patterning

Microfluidic devices have been fabricated to deliver various growth factors and dyes across cells and cell surfaces.[92] This technique relies on the controlled, laminar flow of fluids through channels of defined geometry. Microchannels are often formed by contacting PDMS with a substrate or by creating channels in the PDMS itself. These channels can selectively direct biomolecules to specific sites on a substrate to enable cellular adhesion and interaction. Moreover, two or more laminar streams flown in parallel can be combined into a single stream with limited mixing (only slight diffusion at the interface occurs). This is advantageous for patterning cellular environments and for studying subcellular processes.[93] Other desirable attributes of microfluidics are that they are easily fabricated and widely available which in turn makes them a cost effective alternative.[34]

Lee et al.[94] recently developed a microfluidic patterning technique based on capillary action through microchannels. This platform is based upon the principle that it is easier to move fluid through a narrow opening due to surface tension and it was employed in the patterning of multiple cell types in a laterally open microchannel. The microfluidic device was comprised of a PDMS layer with channels that have walls shorter in height than the layer's edges. Once set, the PDMS layer was positioned atop a glass slide that is coated with PDMS and both the slide and the layer have been plasma treated to increase hydrophilicity. The PDMS layer made a tight seal with the treated glass slide to create a combination of deep and shallow (height = 20–60 μm) open channels. In some instances, polystyrene dishes, rather than PDMS coated glass was used as the base substrate. Preferential fluid movement was expected in the shallow channels allowing for patterning in these areas of an extracellular matrix, poly-L-lysine (PLL), and fibroblast or HeLa cells (Fig. 7). The authors were able to construct several device geometries for the co-culture of cells demonstrating the efficacy of a simple capillary method for such use. This work has applications in generating complex microenvironments for the study of cellular behavior in human disease and diverse ecologies.

SAMs of alkanethiolates on gold have been utilized to attach biomolecules and cells for the study of cell/biomolecule material interactions.[95] Koepsel et al.[96] employed microfluidic techniques to create a SAM-based stem cell culture substrate with discrete patterned areas that varied in terms of ligand identity and density. Here a "localized SAM replacement" approach was carried out to generate the patterned platform via passive pumping which utilized differences in surface tension across the microchannel to drive fluid transport.

Prior to microfluidic processing, a SAM of hydroxyl-terminated oligo(ethylene glycol) (OEG) alkanethiolate was attached to a gold slide via physisorption. At this point, a microfluidic device comprised of several channels was placed atop the preformed SAM. Regions of the preformed SAM are then removed by the flow of $NaBH_4$ over the surface. New SAMs were formed via the flow of aqueous solutions carboxylic acid and hydroxyl terminated OEG alkanethiolate through the microchannels as these molecules interact with the regions exposed from the $NaBH_4$ flow. The final step in the production of the cell culture substrate was the sequential flow of an "activating" solution and a peptide solution through the microchannels to facilitate the covalent attachment of various concentrations of Arg-Gly-Asp-Ser-Pro (RGDSP), an amine-terminated cell adhesion peptide. After substrate generation, human mesenchymal stem cells (hMSCs) were seeded on the substrate. Results demonstrate that hMSCs preferentially attached to areas patterned with RGDSP and that peptide identity and density impact hMSC spreading as well as focal adhesion density. This method allows for the rapid creation of stem culture environments and has applications as a high-throughput screening tool for exploring the influence of immobilized signals on stem cell behavior and phenotype.

INTERFACIAL GRADIENTS

Numerous interfacial gradients exist in the body, whether it be it physical such as a change in surface roughness at the boundaries of different tissues[97] or electrochemical, such as those involved in the generation of action potentials.[98] In fact, gradients play a critical role in many biological processes such as embryonic development, immune response, tissue regeneration, and tumor metastasis.[99] Therefore, the generation of engineered gradients should provide insight into cell behavior and function in more *in vivo* like conditions. In addition, gradients allow several unique surface conditions to be explored on a single sample saving both time and money.[100] Prior to engineering surface gradients, gradient experiments were often conducted by releasing a molecule from a source and allowing a concentration gradient based on diffusion to form over time. [34] However, this was inefficient as there was instability in this system and it was difficult to control the concentration profile. Today, a plethora of methods exist for creating defined gradients including chemical conversion of SAMs with UV stimuli, immobilization of ligands via photopolymerization, and electrochemical adsorption or desorption of signaling molecules. [101] Some of these chemical gradients are limited in their long-term stability due to the use of materials such as SAMs of alkanethiols which are easily oxidized or by use of physically adsorbed ligands which results in desorption of the ligands over time. In addition to chemical gradients, morphological roughness gradients have also been generated.[102–104] For the purpose of this review we will focus on methods for generating immobilized chemical, microfluidic, plasma polymer, morphological, and hydrogel gradients for biological applications.

Immobilized Chemical Gradients

Biomolecules may be attached to surfaces to create continuous and discrete gradients for investigating cell–material interactions.[105,106] These molecules may be attached via physical adsorption or by covalent means. However, covalent immobilization affords greater control over the orientation of the biomolecules, and since orientation is known to influence function, covalent immobilization is preferred. Therefore, several gradients, which incorporate covalent immobilization strategies will be highlighted herein. Harris et al., modulated polymer brush density to influence subsequent immobilization of the cell adhesion peptide RGD which in turn impacted fibroblast adhesion to the polymer brush.[107] In particular, a photoinitiator was deposited onto a silicon wafer and then a methacrylic acid (MAA) monomer was added to the treated substrate. The sample was irradiated with variable exposure times but with constant intensity across the substrate to generate a polymer chain density gradient. Initially, the anionic brush was resistant to cell adhesion and was therefore functionalized to promote fibroblast adhesion. Further functionalization of the PMAA surface involved conjugation of the RGD ligand to the polymer brush via appropriate surface chemistries. Once the gradient was prepared, 3T3 mouse fibroblasts were seeded onto the gradient surfaces and cell adhesion was assessed as a function of ligand density. Results indicate that the RGD surface concentration increased with polymer brush thickness (which increased with increasing irradiation time). Cell adhesion was also found to increase as ligand density increased. Applications of this work include wound healing and nerve regeneration.

Peptide concentration gradients were also generated via SAM and click chemistry.[108] In this work, Moore et al., used vapor deposition to coat glass coverslips with an octyldimethylchlorosilane SAM. Coverslips were attached to a motorized stage and exposed to UV with increasing exposure times resulting in increased SAM oxidation and thus a gradient in surface energy across the surface. A polyethylene oxide (PEO) linker was covalently coupled to the oxidized SAM surface via click chemistry and then this PEO linker served as the recognition moiety for an osteogenic growth peptide (OGP). Osteoblasts were seeded onto the surfaces and behavior observed over a 24 h time period. At all-time points, gradient surfaces with OGP were found to have enhanced cell density and proliferation as compared to controls of gradient-only and smooth surfaces. Gradients compatible with click chemistry may also be generated by chemical vapor deposition polymerization (CVD).[109] More recently, CVD copolymer gradients have been used to control cellular transduction of human gingival fibroblasts by covalent immobilization of a cell-signaling adenovirus.[110]

Additionally, gradients can be generated by ink jet printing techniques.[111] In this instance, Yamazoe et al. used ink jet printing to make gradients of polyethylenimine (PEI) on an albumin based-substrate. PEI solution was placed into the ink jet cartridge and distributed across the surface in a gradient of increasing PEI concentration. L929 mouse fibroblast cells were then seeded onto the gradient. Cell adhesion

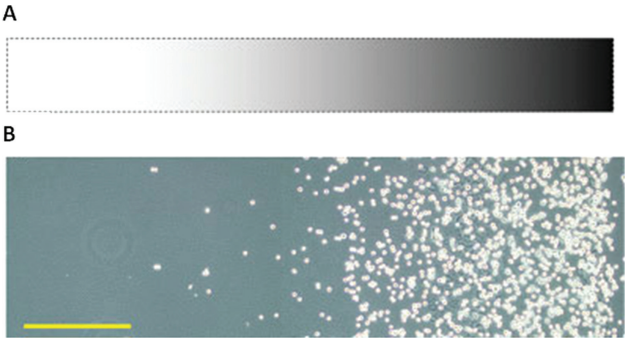

FIGURE 8 PEI gradient and corresponding cellular response. (a) Gradient pattern depicted by computer software in increasing concentrations of PEI (left to right). (b) Mouse fibroblast gradient after cell seeding. (Scale bar = 500 μm).[111]

increased as a function of increasing PEI surface density with no cells adhering to low density regions and large numbers of cells adhering to the high-density regions (Fig. 8). This gradient approach can also be utilized to study the influence of ligand interactions on cell behavior.

Microfluidic Techniques for Interfacial Gradients

Several authors have indicated the utility of microfluidics for gradient generation in the study of cell chemotaxis,[112] neuronal development,[113] and embyrogenesis.[114] Flows can be controlled to the extent that only a portion of the cell interacts with a given flow. For example, Takayama et al.[36] demonstrated that by placing a cell at the interface of two streams, one could expose the cell to multiple microenvironments. Specifically, the authors were able to deliver small molecules to selected cellular domains. This technique, called partial treatment of cells using laminar flows, would be particularly useful in investigating how various soluble factors influence the cellular microenvironment.

Utilizing gradients to study neuronal cells is particularly attractive. However, one of the major challenges in using gradients in neural cell research is the ability to make chemical gradients on the large scale, several hundred micrometers, in which these cells function. Dertinger et al.[115] addressed this issue, by using microfluidics to create protein-gradients. In this instance, the authors used this approach to orient neuron axons. However, the method is generally applicable for the creation of biomolecular gradients. Specifically, a linear concentration gradient of 250 μm comprised of bovine serum albumin and laminin was created on PLL. The gradient was generated by two inlets and four or five serpentine streams that formed a step-profile wherein each stream contained different concentrations of protein. Mixing occurs in the serpentine channels and then all the streams exit via a single outlet and are delivered across the PLL coated microfluidic channel (Fig. 9). Once the protein gradient was created, neuronal cells were cultured on the gradient surface and the direction of axonal growth observed. The authors found axonal growth occurred preferentially in the direction of increasing laminin concentration. Neuronal cell behavior on gradients has also been explored by creating protein concentration gradients modulated by the grafting density of a poly(acylic acid) (PAA) polymer.[116]

Mixed monolayer gradients of alkanethiol SAMs have been utilized to create patterned cell co-cultures and to investigate the dynamics of cell migration.[117] In this work, SAM patterns were rapidly created via microfluidic lithography (μFL). Specifically, a PDMS microfluidic cassette with a spiral pattern was placed atop bare gold and hexadecanethiol (HDT) flown across the surface with the aid of negative pressure at the outlet. The flow duration and concentration of alkanethiol influenced the pattern dimensions with extended flows and higher concentrations leading to larger feature sizes. Thus gradients of pattern sizes were created on the same surface. After μFL, the unpatterned areas of the substrate were backfilled with other alkanethiols, in this case a tetra(ethylene glycol)-terminated undecanethiol, to generate surface architectures of increasing complexity. Once patterned, fibronectin was adsorbed as a cell adhesive monolayer to the hydrophobic HDT areas. To study the dynamics of cell migration, a PDMS mask covered part of the patterned surface and fibroblasts were seeded onto the mixed SAM layer via centrifugation. Then the mask was removed and cells selectively migrated to the cell adhesive regions, that is, the HDT patterned areas. Co-cultures were also created using the same procedure, with an additional centrifugation of the second cell line and removal of the PDMS mask. The two cell populations were distinguished by a fluorescent dye (Fig. 10). This work has applications as a tool for a wide range of cell migration and intercellular communication studies. Nonetheless, the use of SAMs of alkanethiolates in this instance limits the universal application of this approach as these SAMs have been known to desorb from surfaces when exposed to biological media with and without serum during prolonged culture.[118] Furthermore, the SAM's functional end group as well as the type of cells utilized also influences SAM stability over time as SAMS may be degraded or desorbed from the surface.[119] Degradation or desorption may

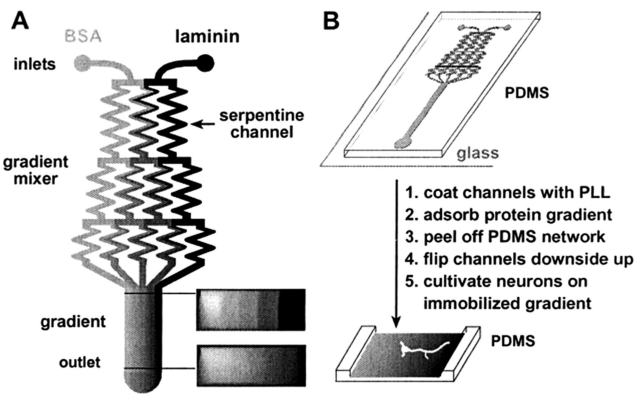

FIGURE 9 Schematic of PDMS microfluidic device for fabricating ligand gradients. (a) Different concentrations of protein were injected into each stream and then stream pooled into a single outlet. (b) Step-by-step process for creating the gradient and subsequent neuronal cell culture.[115]

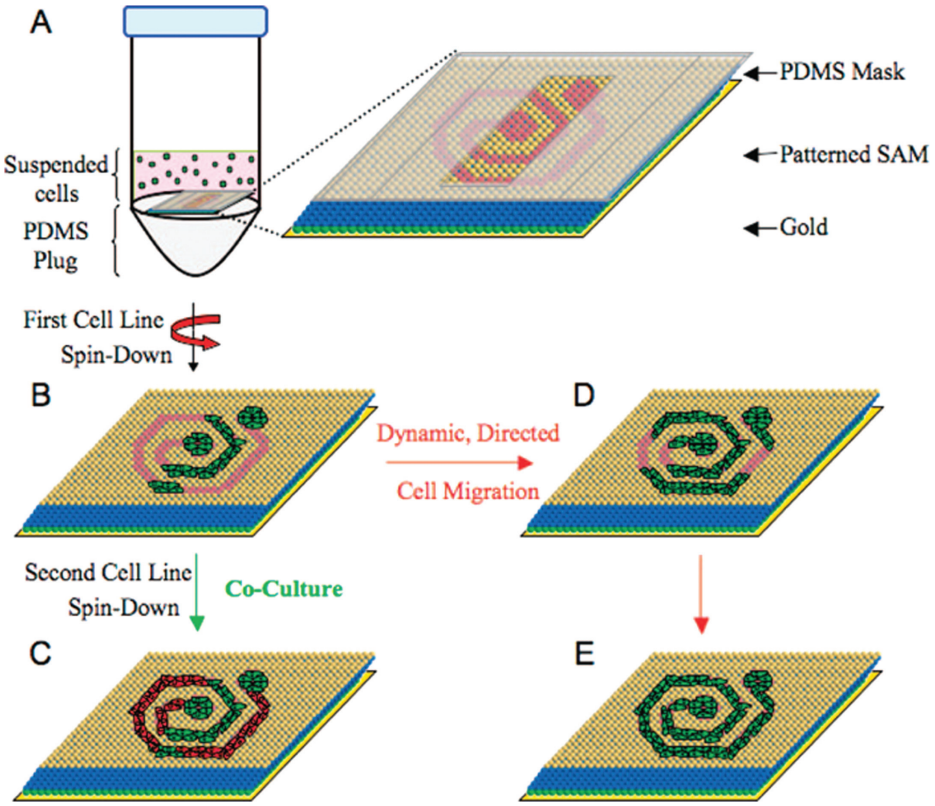

FIGURE 10 Microfluidic lithography and centrifugation were used in conjunction to produce co-culture surfaces that could direct cell motility and growth. The step-by-step process was as follows: (a) Selectively masked patterned substrates placed into centrifuge tube with cells. (b) Cells selectively attached to patterned region after first spin down. (c) Second spin down and removal of mask used to create patterned co-cultures. (d and e) Surfaces for directed cell growth and migration generated by mask removal and allowing cells to access newly unveiled pattern adhesive regions.[117]

occur as a result of oxidation, synthesis defects, or liquid immersion.[120–122]

The advantage of microfluidic gradients lies in the ability to study cellular processes on a small scale reducing the number of cells and reagents needed to conduct an experiment. However, the size of the devices limits the type of substrate that can be patterned with this approach. Moreover, this advantage is also a limitation for this method, because it cannot be used to investigate phenomena with commonly utilized biological tools such as cell culture dishes and plates. Though microfluidic gradients may be too small for some uses, they are also too large for others as phenomena that are apparent on the nanoscale may not be readily detectable at the microscale.

Plasma Polymer Techniques for Interfacial Gradients

Plasma polymerization, the generation of polymeric materials under the influence of ionized gas (plasma), may also be used to create gradient surfaces.[123] These polymers arise from the glow discharge which is excited from an organic precursor gas and flown into a reactor under reduced pressure and at a controlled rate.[124] This approach can generate a wide range of surface chemistries and can be applied in the modification of most substrates due to its formation of well adhered surface layers that are pin-hole free. Furthermore, plasma polymerization has demonstrated suitability for clinical applications.[125,126] A commonly utilized method of gradient generation utilizes a mask and is diffusion-based. In this instance, monomer is diffused beneath a solid mask with the distance of the mask from the substrate controlling the plasma film depth and thus the slope of the gradient. Plasma film depth may also be modulated by augmenting the plasma polymerization time. However, the use of this fabrication method may be limited by the need for costly equipment such as the vacuum and reactor system in which the plasma polymerization occurs. In addition, a wealth of process parameters including flow rate, pressure, substrate temperature, input power, and frequency add to the system complexity potentially making it difficult to optimize process parameters.[127]

Harding et al.[128] have used plasma polymerization to investigate the influence of stem cell spreading on stem cell differentiation. For this work, the authors produced a plasma copolymer gradient consisting of diethylene glycol (DG) dimethyl ether and acrylic acid (AA) plasma polymers. The DG plasma polymer was selected because it is a non-fouling or protein resistant material similar to the commonly utilized PEO. Although AA plasma polymers were chosen

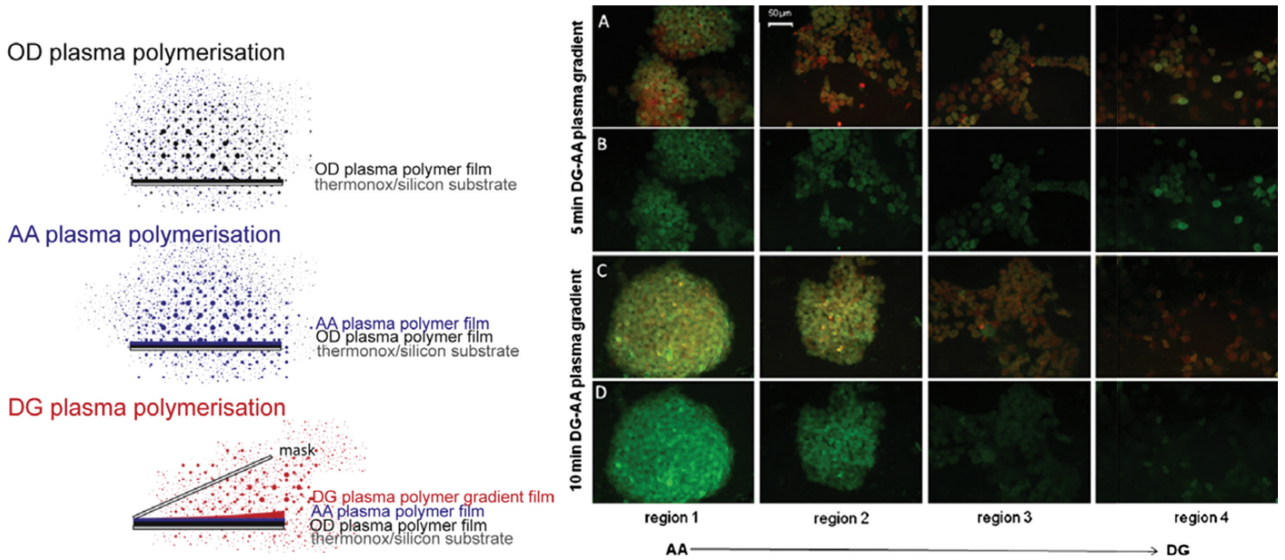

FIGURE 11 Plasma polymer gradients used to study the impact of gradient chemistry on mouse embryonic stem cells. Schematic of plasma polymer layer deposition on silicon (Si) or Thermanox: OD plasma polymer, AA plasma polymer and the final diethylne glycol dimethyl ether (DG) plasma polymer gradient layer (left). Expression of pluripotency marker Oct 4 in ES cell colonies at an intermediate time point (3 days of culture) on 5 min (A, B) and 10 min (C, D) AA–DG plasma polymer gradients. Photomicrographs show heterogeneous Oct4 expression within DG plasma polymer-rich regions. Photomicrographs of colonies representative of each region. Panels A and C show counterstaining of fixed cells with PI, panels B and D, show Oct4 expression alone (right). Scale bar = 50 μm.

because they are known to promote protein and cell adhesion.[129,130] Prior to gradient generation, silicon or Thermanox cell culture treated coverslips were placed in the plasma reactor and an adhesion layer of octadiene (OD) plasma layer was deposited. Then AA plasma polymer was homogenously deposited on the samples. A gradient of DG plasma polymer was then created using a glass slide tilted at an angle of 12° to mask the samples [Fig. 11 (left side)]. Resulting gradients were 3 cm in length and the depth (and thus the slope) of the gradients was augmented by the use of two polymerization times, 5 and 10 min, respectively. At this juncture, mouse embryonic stem cells (mES) were cultured on the gradients and stem cell colony attachment, spreading, morphology, and differentiation were assessed. In general, AA-rich regions of the gradient had greater attachment and spreading which decreased as the amount of DG in the gradient increased irrespective of the treatment time. For both gradient types, stem cell morphology and characteristic expression of stem cell markers (such as Oct 4) was maintained in regions with high DG concentration [Fig. 11 (right side)]. Investigation of serum protein adsorption onto the gradients provided a plausible explanation of this phenomenon; that the cellular response is strongly influenced by plasma film depth which in turn mediated the adsorption of serum proteins onto the gradients.

In addition to generating chemical gradients like that in the previous example, diffusion-based plasma polymerization has also been utilized to create wettability gradients. For example Zelzer et al.,[131] generated a wettability gradient to assess the influence of this surface property on the adhesion and proliferation of NIH 3T3 murine fibroblasts. Here a gradient of a hydrophobic (water contact angle of $\sim 90°$) plasma polymermerized hexane (ppHex) was generated on a hydrophilic (water contact angle of 63°) plasma polymerized allylamine (ppAAm). Glass slides were used as the substrates with both a steep and a shallow gradient being generated by augmenting the distance of the mask from the substrate surface. Cell behavior was assessed on both gradient types and compared to that of homogenously coated substrates. Irrespective of the gradient type, cell adhesion and proliferation was shown to decrease as the concentration of ppHex increased. Cell adhesion and proliferation on the ppHex end of the gradient was comparable to that on homogenously coated substrates. However, differences were noted between the steep and shallow gradients as compared to homogenously coated substrates of ppAAm. The number of cells adhered to the ppAm end of the gradient was half that of a homogenously coated substrate irrespective of the gradient steepness. There was no difference in the cellular proliferation rates on gradient and homogenous samples. Zelzer et al. hypothesize that this adhesion disparity may occur due to differences in cell-cell signaling or protein adsorption but note that further investigation is warranted before determining the source of the disparity. Nonetheless, these results indicate the need for validation testing before extrapolating cellular results on homogenous surfaces to that on gradient surfaces.

Additionally, the influence of wettability gradients generated by plasma polymerization on the cellular response of mES cells has been studied. Specifically, the hydrophobic OD

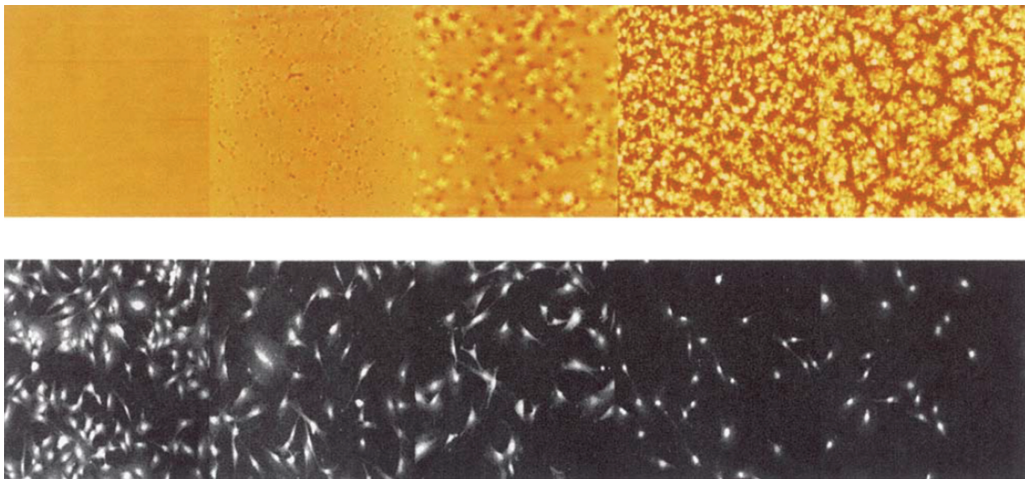

FIGURE 12 Montage of representative images of PLLA morphology from AFM data (top panels, field of view in each image is 20 mm), and corresponding cell count from fluorescent microscopy (bottom panels, field of view in each image is 1500 mm).[144]

plasma polymer and the hydrophilic AA plasma polymer were used to create a wettability gradient to study the influence of this surface property on mES cell spreading and differentiation. The resulting wettability gradient on Thermanox cell culture slides had static water contact angles that ranged from 47° to 88° from the AA to the OD ends respectively. Different media and different mES cell lines were assessed to determine what influence the gradient had on the resultant stem cell behaviors. Irrespective of the stem cell or media type, cell colony number and size were found to increase with increasing concentration of AA up to a certain point; though the location of the maximum colony number and size differed based on the cell and media type. Cell differentiation, as shown by the presence of a common ES cell marker, alkaline phosphotase, was also evaluated. Results indicate that colonies of intermediate size (less than or equal 120 μm^2) colonies were primarily comprised of undifferentiated cells as evidenced via fluorescence intensity while those larger than this were more differentiated. Thus, in this instance it is the colony size, and not the surface chemistry directly that has a greater influence on stem cell behavior.

Morphological Gradients

Surface roughness, protrusions and/or depressions found on the uppermost layer of a material, have been shown to impact cell adhesion,[132] proliferation,[133] and differentiation.[134] As a result, surface roughness has been incorporated into orthopedic implants like hip replacements to facilitate osseointegration[135] and into periodontal implants to enhance the proliferation and differentiation of cells surrounding an implant site.[136] Roughness gradients exist *in vivo* and thus to systematically investigate cell–material interactions in response to such gradients, synthetic analogs need to be generated. A myriad of techniques have been utilized to create morphological gradients including particles,[137,138] erosion/chemical polishing,[139] polymer blending,[140] and polymer temperature gradients.[141,142] These techniques have resulted in gradients of various dimensions (nano- and microscale) and geometries. Of the aforementioned techniques, the use of particles is the most prevalent. For example, Kunzler et al.[143] used positively charged poly(ethylene imine) (PEI)-coated silicon wafers to attach negatively charged silica particles to create morphological gradients on the nano-scale. The particles were surface modified via sintering at 1125 °C where sintering time was used to modulate particle spacing along the wafer with an increase in sintering time corresponding to a decrease in particle spacing. As a result, a particle density gradient and thus a surface roughness gradient, was produced. Rat rat calvarial osteoblasts (RCO) were cultured on the roughness gradients and the impact of the gradient on cell morphology and proliferation was assessed.[143] In general, RCO proliferation increased as particle spacing and thus surface roughness decreased after 4 and 7 days of culture. This study noted the same trend for cell morphology, with cells being more spread out in areas displaying reduced surface roughness.[143]

Another attempt at investigating the influence of nanoscale roughness gradients was completed by Washburn et al.[144] In this instance, a polymer temperature gradient was employed that exploited changes that occur in the roughness of a polymer as a function of changes in the polymer crystallinity. Specifically, 3% poly(L-lactic acid) (PLLA) in chloroform was adhered to silicon wafers (note that the wafers had been pre-treated to make the surface hydrophobic for enhanced PLLA adhesion). Then, the PLLA-coated substrates were annealed on a custom-built temperature gradient stage with limits of 44 and 100 °C respectively. Annealing treatments resulted in a root mean square surface roughness gradient that ranged between 0.5 and 13 nm. Proliferation of osteoblastic MC3T3-E1 cells as a function of gradient roughness was examined and as in the previous study, an increase in nanoscale surface roughness was shown to reduce cell proliferation over a 5-day period (Fig. 12). To demonstrate that changes in proliferation were purely associated with changes in surface roughness, and not serum protein adsorption, an assay for the adsorption of fibronectin and vitronectin was undertaken. Results indicated no significant influence of

protein adsorption and thus proliferation changes were attributed to changes in surface roughness. However, the interpretation of the results of this study are complicated because in addition to changing surface roughness, the shape of the surface features also changed and this has been shown to impact cell behavior.[145]

As both micro- and nanoscale roughness features are known to influence cell phenotype and function,[146] a recent study looked at the synergistic effects of a surface having a combination of micro- and nanoscale roughness.[147] Briefly, a microscale roughness gradient was incorporated onto the surface of an aluminum sheet by sandblasting followed by polishing via immersion in a chemical polishing solution. The generated gradient ranged from 0.8 to 4.1 μm in average roughness (R_a). This surface was further modified by dipping it into a nanoparticle solution and then removing it incrementally to generate a nanoscale particle density gradient on the order of 0 to 74 particles per μm^2. MC3T3 osteoblasts were cultured on the cells for 14 days in an osteogenic media and then assessed in terms of their expression of an osteogenic marker, osteopontin. Highest expression was found on surfaces that combined highest microscale roughness with an intermediate nanoparticle density (30–40 particles/μm^2).

3D Gradients in Hydrogels

Up to this point, a majority of our discussion has centered on gradients in 2D. However, cells exist in a complex 3D environment and thus the influence of gradients on cellular behavior should also be evaluated in 3D. A majority of the gradient work in 3D thus far has been generated through the use of hydrogels. Several methods are utilized to generate gradients in hydrogels, though the use of microfluidic devices is most prevalent.[148–150] Gradients involving the use of hydrogels for cellular studies may be classified as: 1. 3D hydrogel gradients with cell studies conducted on the surface of the hydrogel 2. 3D hydrogel gradients with cell studies conducted within the hydrogel.

Typically work has been done on the surface of gradient hydrogels.[151–154] For example, a poly(ethylene glycol)-diacrylate (PEGDA) hydrogel with a surface gradient of the adhesion peptide RGD was designed to assess the effects of concentration gradients on the adhesion and spreading of rat bone marrow-derived mesenchymal stem cells (rMSCs).[148] The gradient was fabricated by injecting a hydrogel precursor solution with or without RGD-conjugation into a microfluidic gradient generator. In the presence of a photoinitiator, PEGDA conjugated RGD was crosslinked via photo-polymerization. The existence of RGD gradients was confirmed by fluorescence microscopy as the hydrogel had been labeled with fluorescein isothiocyanate (FITC). After producing gradients varying in steepness, rMSCs were cultured on the hydrogel surfaces and cell adhesion and spreading were evaluated. In general, the number of cells adhered and degree of cell spreading increased with increasing RGD concentration up to a saturation point. This effect was more pronounced on steeper gradients than on shallow gradients.

Another example of cellular studies conducted on the surface of a 3D hydrogel involved a molecular concentration gradient which was initiated by a passive pump induced forward flow and extended further via an evaporation-induced backward flow in a microfluidic channel.[155] The materials used to generate the gradient include photocrosslinkable hydrogel precursors (a combination of photoinitiator, poly(ethylene glycol)-diacrylate (PEG-DA), and/or a PEG-derivative of the cell adhesive ligand RGD). By altering the concentration of the hydrogel precursors, a chemical gradient on the centimeter length scale could be generated and stabilized once the hydrogel was crosslinked via UV exposure. Cell–material interactions were assessed via the culture of human umbilical vein endothelial cells on the gradient hydrogels. Cells were more numerous and spread out better on portions of the chemical gradient that had higher concentrations of the cell adhesive ligand RGD. This work has applications in the generation of long-range gradients for cell migration experiments.

In addition to surface cues provided by soluble and immobilized factors, cellular cues may also be provided by surface stiffness impacting cellular adhesion, migration, morphology, and function.[156–158] As such, gradients in hydrogel stiffness have also been evaluated to determine the influence of this property on hMSC migration and differentiation.[159] Hydrogels were comprised of poly(acrylamide) and the stiffness of the hydrogels, as indicated by the corresponding elastic modulus, was augmented via the incorporation of a photoinitiator and UV exposure. In particular, a UV light was shone through a gradient photo mask such that some areas received more exposure than others resulting in a gradation in the hydrogel stiffness. The elastic modulus of the gradient hydrogel ranged between 1 and 14 kPa and the slope of the gradient was on the order of 1.0 ± 0.1 kPa/mm as determined by AFM. hMSC migration and differentiation was assessed over the course of 21 days. By day 21, hMSCs were found to migrate in the direction of greater stiffness and as they did so, began to differentiate down a myogenic lineage where differentiation was indicated by immunohistochemistry (Fig. 13). Results of this study may lead to the assessment of stiffness changes rather than static stiffness alone. Though promising, the aforementioned as well as other hydrogel gradient studies are limited because the actual cell analysis still occurred on the surface rather than within the 3D hydrogel matrix.[160]

Few studies have evaluated the cellular response of cells within a 3D gradient hydrogel.[160–162] One such study was conducted by Dodla and Bellamkonda and was used to assess neurite extension for applications in nerve regeneration.[163] In this work, a growth promoting glycoprotein, laminin-1 (LN-1) was incorporated into a 3D agarose hydrogel. The agarose hydrogel was placed in a chamber where one side was exposed to a concentrated solution of LN-1 (high concentration compartment) and the other side was exposed to phosphate buffered saline (low concentration compartment). Diffusion of the LN-1 across the gel from the high concentration compartment toward the low concentration compartment occurred over the course of 6 h and then was photocrosslinked via UV light. Because the LN-1 was

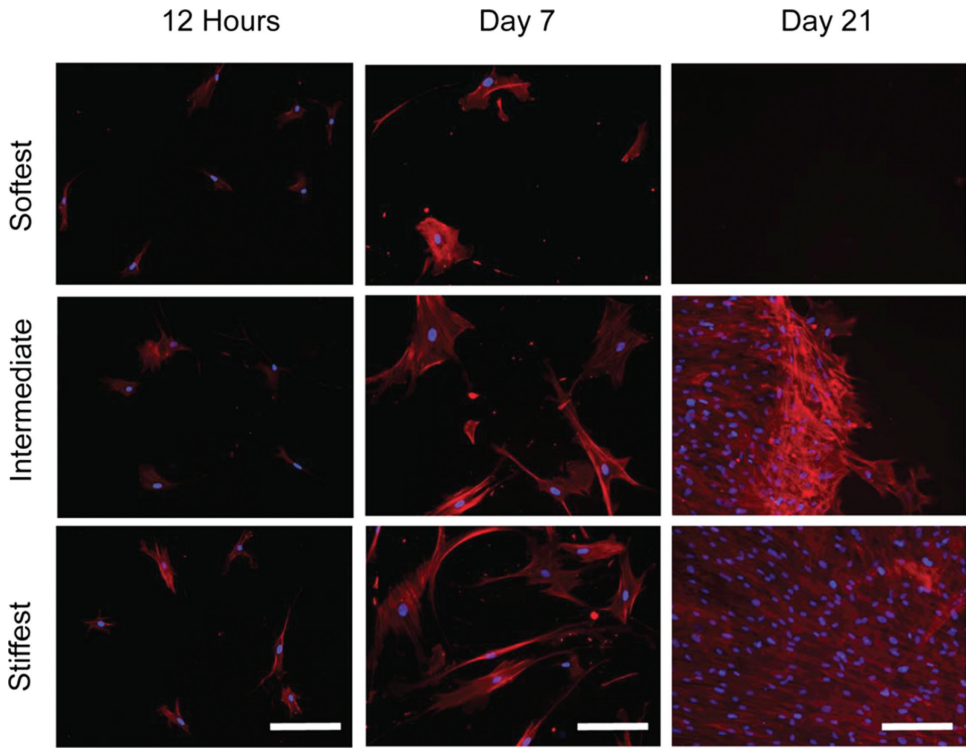

FIGURE 13 Spatial distribution of mitomycin C-treated MSCs on gradient hydrogels. Images of Hoescht 33342 (blue) and phalloidin (red)-stained mitomycin C-treated MSCs plated at low density (250 cells/cm^2) illustrate the change in distribution with time. After 21 days, MSCs are locally confluent in the stiffest region of the hydrogel. Scale bar is 56.5 mm.[159]

fluorescently labeled, the persistence of the gradient through the various layers of the 3D network could be assessed. Once a uniform gradient was confirmed via fluorescence microscopy, cellular assessments could begin. The gradient set-up for the cell tests was the same as that previously described with the exception that dorsal root ganglia (DRG) from chicken embryos were suspended in the agarose gel prior to LN-1 exposure and that DMEM was used in the low concentration compartment. Neurite outgrowth from the DRGs was assessed over a 4 day period with slopes of the LN-1 concentration gradients ranging from 0.017 to 0.121 μg/mL/mm. Fastest growth rates were seen for the gradient with the mildest slope (0.017 μg/mL/mm). At this point, the fastest neurite outgrowth on gradient gels was compared to that of isotropic gels, and neurite outgrowth was shown to be significantly faster on gradient scaffolds. Results of this work may be used to facilitate peripheral nerve regeneration *in vivo*.

Microspheres containing growth factors have also been incorporated into 3D hydrogels to create chemical gradients.[164] For this work, salt leaching was used to generate pores in a water-based silk fibroin scaffold, with the pore size being defined by the size of the salt crystals utilized. Silk microspheres containing recombinant bone morphogenic protein 2 (rhBMP-2) and/or recombinant insulin-like growth factor I (rhIGF-I) were then encapsulated in the scaffold using a gradient generator. The generator consisted of two adjacent chambers which contained the same concentration of hMSCs but different concentrations of silk microspheres within the silk fibroin. A valve separating the chambers was opened and a peristaltic pump was used to create a gradient as the solution from the first chamber was mixed with an increasingly lower volume of solution within the second chamber. This mixed solution was eluted into a single chamber containing the salt particle solution which was used to generate a pores within the gel scaffold. From this process, three distinct scaffold types were produced: 1. Scaffold with rhBMP-2 gradient only 2. Scaffold with rhIGF-I gradient only 3. Scaffold with a dual gradient of rhBMP-2 and rhIGF-I (with increasing concentrations of rhBMP-2 along the length of the gradient). Gradient generation within the scaffolds was determined sectioning the scaffolds and quantifying the amount of rhBMP-2 and rhIGF-I at various scaffold sections using enzyme-linked immunosorbent assay. Once gradient generation had been confirmed, the scaffolds were used to induce the osteochondral differentiation of human bone marrow-derived mesenchymal stem cells (hMSCs). hMSCs were cultured for 5 weeks within the scaffold in a medium containing osteogenic and chondrogenic components. At this juncture, scaffolds were sectioned such that cell differentiation at various points on the concentration gradient could be assessed. In particular, calcium content and histological staining were used to ascertain the extent of hMSC differentiation into an osteochondral lineage as a function of gradient position. Though differentiation was not observed on the rhIGF-I only scaffolds, differentiation was apparent on the rhBMP-2 only scaffolds in the direction of increasing rhBMP-2

concentration. Additionally, the differentiation of hMSCs was enhanced on the dual gradient as compared to the rhBMP-2 gradient alone.

SUMMARY AND OUTLOOK

A plethora of methods have been generated for patterning surfaces and creating surface gradients in order to assess cell–surface interactions. These methods vary in terms of the materials utilized (from polymers to metals) and the complexity of the instrumentation employed to implement these strategies, all of which have been described in this review. The effects of various topographical patterns and gradients on the micro- and nanoscale have been evaluated on a multitude of cell types for diverse applications. This in itself represents advancement in the field as enhanced processes have enabled investigation at smaller length scales. Repeatedly, the researchers highlighted herein have patterned ligands (proteins, peptides, growth factors, etc.) that have an affinity for the cells in question and are used to spatio-selectively control cell adhesion and proliferation. Often, higher ligand density and/or concentrations result in greater cell adhesion and proliferation (up to some plateau point). A similar result is realized for biomolecular gradients, with a greater number of cells adhering to or migrating in the direction of increasing biomolecular densities. The converse is typically true for morphological gradients like roughness gradients, with increasing roughness often being correlated with a decrease in cell adhesion and proliferation for several cell types though differential outcomes may be noted when stem cell differentiation is assessed. Patterning results that look at the influence of pattern spacing and size are inconclusive for several cell lines and types as a certain pattern size or spacing may promote one behavior for one cell type while promoting a different behavior on another. Thus, it is difficult to predict cell behavior on materials due to synergistic effects between material properties and patterning/gradient properties such as ligand concentration, shape, size, and spacing which may lead to divergent outcomes between and among different cell types. As a result, combinatorial approaches should be investigated to enhance our understanding of these interactions. Though engineers and scientists are capable of investigating cell-surface interactions on the micro- and nanoscale, the resolution of many of the techniques is hampered by environmental factors and the long-term stability of some of the materials utilized is questionable for prolonged cell studies as they may be degraded or desorbed from the material surface as a result of oxidation, synthesis defects, and/or immersion in liquids. Furthermore, some of the strategies are cumbersome and do not readily lend themselves to high-throughput investigations. Additionally, the ability to generate more complex surface architectures via simultaneous patterning of multiple ligands is limited. Moreover, there is additional work to be done as several of the methods for patterning and gradient generation are only applicable for planar substrates, which does not accurately mimic the 3D cellular microenvironment. Going forward, the use of combinatorial gradients such as those demonstrating micro- and nanoscale roughness or those consisting of chemical and morphological gradients warrant systematic investigation as some of these properties may interact synergistically to influence cell behavior. To date, patterning and gradient generation have shown great promise in enhancing our understanding of cell responses to physical and chemical cues in the cellular microenvironment.

ACKNOWLEDGMENTS

A.M.R. would like to acknowledge support from the University of Michigan Rackham Predoctoral Fellowship and the Whitaker International Scholars Fellowship program. J.L. acknowledges support from the Defense Threat Reduction Agency under award number is HDTRA1-12-1-0039.

REFERENCES AND NOTES

1 K. von der Mark, J. Park, S. Bauer, P. Schmuki, *Cell Tissue Res* **2010,** *339*, 131–153.

2 H. Geckil, F. Xu, X. H. Zhang, S. Moon, U. Demirci, *Nanomedicine* **2010,** *5*, 469–484.

3 D. Paripovic, H. Hall-Bozic, H. A. Klok, *J. Mater. Chem.* **2012,** *22*, 19570–19578.

4 E. Martinez, A. Lagunas, C. A. Mills, S. Rodriguez-Segui, M. Estevez, S. Oberhansl, J. Comelles, J. Samitier, *Nanomedicine* **2009,** *4*, 65–82.

5 T. Blattler, C. Huwiler, M. Ochsner, B. Stadler, H. Solak, J. Voros, H. M. Grandin, *J. Nanosci. Nanotechnol.* **2006,** *6*, 2237–2264.

6 M. Arnold, V. C. Hirschfeld-Warneken, T. Lohmueller, P. Heil, J. Bluemmel, E. A. Cavalcanti-Adam, M. Lopez-Garcia, P. Walther, H. Kessler, B. Geiger, J. P. Spatz, *Nano Lett.* **2008,** *8*, 2063–2069.

7 C. J. Bettinger, R. Langer, J. T. Borenstein, *Angew. Chem. Int. Ed. Engl.* **2009,** *48*, 5406–5415.

8 J. D. Wu, Z. W. Mao, H. P. Tan, L. L. Han, T. C. Ren, C. Y. Gao, *Interface Focus* **2012,** *2*, 337–355.

9 K. M. Scully, M. G. Rosenfeld, *Science* **2002,** *295*, 2231–2235.

10 D. Julthongpiput, M. J. Fasolka, W. H. Zhang, T. Nguyen, E. J. Amis, *Nano Lett.* **2005,** *5*, 1535–1540.

11 R. A. Potyrailo, L. Hassib, *Rev. Sci. Instrum.* **2005,** *76*, 062225.

12 S. Y. Chen, L. M. Smith, *Langmuir* **2009,** *25*, 12275–12282.

13 O. Akbulut, A. A. Yu, F. Stellacci, *Chem. Soc. Rev.* **2010,** *39*, 30–37.

14 T. F. Didar, A. M. Foudeh, M. Tabrizian, *Anal. Chem.* **2012,** *84*, 1012–1018.

15 L. J. Millet, M. E. Stewart, R. G. Nuzzo, M. U. Gillette, *Lab Chip* **2010,** *10*, 1525–1535.

16 D. Wright, B. Rajalingam, J. M. Karp, S. Selvarasah, Y. B. Ling, J. Yeh, R. Langer, M. R. Dokmeci, A. Khademhosseini, *J. Biomed. Mater. Res. Part A* **2008,** *85A*, 530–538.

17 R. Fishler, A. Artzy-Schnirman, E. Peer, R. Wolchinsky, R. Brener, T. Waks, Z. Eshhar, Y. Reiter, U. Sivan, *Nano Lett.* **2012,** *12*, 4992–4996.

18 H. Y. Chen, M. Hirtz, X. P. Deng, T. Laue, H. Fuchs, J. Lahann, *J. Am. Chem. Soc.* **2010,** *132*, 18023–18025.

19 J. D. Hoff, L. J. Cheng, E. Meyhofer, L. J. Guo, A. J. Hunt, *Nano Lett.* **2004,** *4*, 853–857.

20 X. Z. Ye, L. M. Qi, *Nano Today* **2011,** *6*, 608–631.

21 W. Dai, Y. Z. Zheng, K. Q. Luo, H. K. Wu, *Biomicrofluidics* **2010,** *4*, 024101.

22 X. R. Li, M. R. MacEwan, J. W. Xie, D. Siewe, X. Y. Yuan, Y. N. Xia, *Adv. Funct. Mater.* **2010,** *20*, 1632–1637.

23 E. D. Miller, J. A. Phillippi, G. W. Fisher, P. G. Campbell, L. M. Walker, L. E. Weiss, *Comb. Chem. High Throughput Screen.* **2009,** *12*, 604–618.

24 X. L. Guo, C. G. Elliott, Z. Q. Li, Y. Y. Xu, D. W. Hamilton, J. J. Guan, *Biomacromolecules* **2012,** *13*, 3262–3271.

25 M. Kim, T. Kim, *Anal. Chem.* **2010,** *82*, 9401–9409.

26 P. Y. Wang, W. B. Tsai, N. H. Voelcker, *Acta Biomater.* **2012,** *8*, 519–530.

27 A. Ranella, M. Barberoglou, S. Bakogianni, C. Fotakis, E. Stratakis, *Acta Biomater.* **2010,** *6*, 2711–2720.

28 B. Joddar, Y. Ito, *J. Mater. Chem.* **2011,** *21*, 13737–13755.

29 L. Xu, L. Robert, O. Qi, F. Taddei, Y. Chen, A. B. Lindner, D. Baigl, *Nano Lett.* **2007,** *7*, 2068–2072.

30 X. K. Lin, Q. He, J. B. Li, *Chem. Soc. Rev.* **2012,** *41*, 3584–3593.

31 S. Gilles, C. Kaulen, M. Pabst, U. Simon, A. Offenhausser, D. Mayer, *Nanotechnology* **2011,** *22*, 295301.

32 A. P. Quist, S. Oscarsson, *Exp. Opin. Drug Discov.* **2010,** *5*, 569–581.

33 D. Falconnet, G. Csucs, H. M. Grandin, M. Textor, *Biomaterials* **2006,** *27*, 3044–3063.

34 A. Khademhosseini, R. Langer, J. Borenstein, J. P. Vacanti, *Proc. Natl. Acad. Sci. USA* **2006,** *103*, 2480–2487.

35 N. Patel, R. Padera, G. H. W. Sanders, S. M. Cannizzaro, M. C. Davies, R. Langer, C. J. Roberts, S. J. B. Tendler, P. M. Williams, K. M. Shakesheff, *FASEB J.* **1998,** *12*, 1447–1454.

36 S. Takayama, E. Ostuni, P. LeDuc, K. Naruse, D. E. Ingber, G. M. Whitesides, *Nature* **2001,** *411*, 1016–1016.

37 C. S. Chen, M. Mrksich, S. Huang, G. M. Whitesides, D. E. Ingber, *Science* **1997,** *276*, 1425–1428.

38 C. Vieu, F. Carcenac, A. Pepin, Y. Chen, M. Mejias, A. Lebib, L. Manin-Ferlazzo, L. Couraud, H. Launois, *Appl. Surf. Sci.* **2000,** *164*, 111–117.

39 Y. N. Xia, G. M. Whitesides, *Annu. Rev. Mater. Sci.* **1998,** *28*, 153–184.

40 A. Perl, D. N. Reinhoudt, *J. Adv. Mater.* **2009,** *21*, 2257–2268.

41 C. C. Wu, D. N. Reinhoudt, C. Otto, V. Subramaniam, A. H. Velders, *Small* **2011,** *7*, 989–1002.

42 R. C. Schmidt, K. E. Healy, *J. Biomed. Mater. Res. Part A* **2009,** *90A*, 1252–1261.

43 A. L. Hook, N. H. Voelcker, H. *Acta Biomater.* **2009,** *5*, 2350–2370.

44 C. M. Kolodziej, H. D. Maynard, *Chem. Mater.* **2012,** *24*, 774–780.

45 P. M. Mendes, C. L. Yeung, J. A. Preece, *Nanoscale Res. Lett.* **2007,** *2*, 373–384.

46 C. S. Whelan, M. J. Lercel, H. G. Craighead, K. Seshadri, D. L. Allara, *Appl. Phys. Lett.* **1996,** *69*, 4245–4247.

47 H. Hatakeyama, A. Kikuchi, M. Yamato, T. Okano, *Biomaterials* **2007,** *28*, 3632–3643.

48 F. Kantawong, K. E. V. Burgess, K. Jayawardena, A. Hart, R. J. Burchmore, N. Gadegaard, R. O. C. Oreffo, M. J. Dalby, *Biomaterials* **2009,** *30*, 4723–4731.

49 G. Dos Reis, F. Fenili, A. Gianfelice, G. Bongiorno, D. Marchesi, P. E. Scopelliti, A. Borgonovo, A. Podesta, M. Indrieri, E. Ranucci, P. Ferruti, C. Lenardi, P. Milani, *Macromol. Biosci.* **2010,** *10*, 842–852.

50 D. O. Rodgerson, A. G. Harris, *Stem Cell Rev. Rep.* **2011,** *7*, 782–796.

51 H. Takahashi, M. Nakayama, K. Itoga, M. Yamato, T. Okano, *Biomacromolecules* **2011,** *12*, 1414–1418.

52 V. S. Goudar, S. Suran, M. M. Varma, *Micro Nano Lett.* **2012,** *7*, 549–553.

53 P. Bhatnagar, G. G. Malliaras, I. Kim, C. A. Batt, *Adv. Mater.* **2010,** *22*, 1242.

54 M. J. Brady, A. Davidson, *Rev. Sci. Instrum.* **1983,** *54*, 1292–1295.

55 R. S. Kane, S. Takayama, E. Ostuni, D. E. Ingber, G. M. Whitesides, *Biomaterials* **1999,** *20*, 2363–2376.

56 R. Michel, J. W. Lussi, G. Csucs, I. Reviakine, G. Danuser, B. Ketterer, J. A. Hubbell, M. Textor, N. D. Spencer, *Langmuir* **2002,** *18*, 3281–3287.

57 D. Falconnet, A. Koenig, T. Assi, M. Textor, *Adv. Funct. Mater.* **2004,** *14*, 749–756.

58 K. Jang, Y. Xu, K. Sato, Y. Tanaka, K. Mawatari, T. Kitamori, *Microchim. Acta* **2012,** *179*, 49–55.

59 M. S. Hahn, L. J. Taite, J. J. Moon, M. C. Rowland, K. A. Ruffino, J. L. West, *Biomaterials* **2006,** *27*, 2519–2524.

60 C. A. Scotchford, M. Ball, M. Winkelmann, J. Voros, C. Csucs, D. M. Brunette, G. Danuser, M. Textor, *Biomaterials* **2003,** *24*, 1147–1158.

61 M. Kim, J. C. Choi, H. R. Jung, J. S. Katz, M. G. Kim, J. Doh, *Langmuir* **2010,** *26*, 12112–12118.

62 J. Turkova, *J. Chromatogr. B* **1999,** *722*, 11–31.

63 G. M. Whitesides, E. Ostuni, S. Takayama, X. Y. Jiang, D. E. Ingber, *Annu. Rev. Biomed. Eng.* **2001,** *3*, 335–373.

64 W. Y. Xia, W. Liu, L. Cui, Y. C. Liu, W. Zhong, D. L. Liu, J. J. Wu, K. H. Chua, Y. L. Cao, *J. Biomed. Mater. Res. Part B: Appl. Biomater.* **2004,** *71B*, 373–380.

65 Y. N. Xia, G. M. Whitesides, *Angew. Chem. Int. Ed. Engl.* **1998,** *37*, 551–575.

66 G. Csucs, T. Kunzler, K. Feldman, F. Robin, N. D. Spencer, *Langmuir* **2003,** *19*, 6104–6109.

67 D. Lehnert, B. Wehrle-Haller, C. David, U. Weiland, C. Ballestrem, B. A. Imhof, M. Bastmeyer, *J. Cell Sci.* **2004,** *117*, 41–52.

68 H. Schmid, B. Michel, *Macromolecules* **2000,** *33*, 3042–3049.

69 M. Mayer, J. Yang, I. Gitlin, D. H. Gracias, G. M. Whitesides, *Proteomics* **2004,** *4*, 2366–2376.

70 V. A. Schulte, Y. B. Hu, M. Diez, D. Bunger, M. Moller, M. C. Lensen, *Biomaterials* **2010,** *31*, 8583–8595.

71 T. T. Truong, R. S. Lin, S. Jeon, H. H. Lee, J. Maria, A. Gaur, F. Hua, I. Meinel, J. A. Rogers, *Langmuir* **2007,** *23*, 2898–2905.

72 X. X. Li, S. Hou, X. Z. Feng, Y. Yu, J. J. Ma, L. Y. Li, *Colloids Surf. B:Biointerfaces* **2009,** *74*, 370–374.

73 Y. D. Teng, E. B. Lavik, X. L. Qu, K. I. Park, J. Ourednik, D. Zurakowski, R. Langer, E. Y. Snyder, *Proc. Natl. Acad. Sci. USA* **2002,** *99*, 9606–9606.

74 R. Lovchik, C. von Arx, A. Viviani, E. Delamarche, *Anal. Bioanal. Chem.* **2008,** *390*, 801–808.

75 M. Mrksich, G. M. Whitesides, *Annu. Rev. Biophys. Biomol. Struct.* **1996,** *25*, 55–78.

76 T. A. Petrie, B. T. Stanley, A. J. Garcia, *J. Biomed. Mater. Res. Part A* **2009,** *90A*, 755–765.

77 N. T. Flynn, T. N. T. Tran, M. J. Cima, R. Langer, *Langmuir* **2003,** *19*, 10909–10915.

78 D. L. Wilson, R. Martin, S. Hong, M. Cronin-Golomb, C. A. Mirkin, D. L. Kaplan, *Proc. Natl. Acad. Sci. USA* **2001,** *98*, 13660–13664.

79 G. Agarwal, L. A. Sowards, R. R. Naik, M. O. Stone, *J. Am. Chem. Soc.* **2003,** *125*, 580–583.

80 D. S. Ginger, H. Zhang, C. A. Mirkin, *Angew. Chem. Int. Ed. Engl.* **2004,** *43*, 30–45.

81 C. L. Cheung, J. A. Camarero, B. W. Woods, T. W. Lin, J. E. Johnson, De J. J. Yoreo, *J. Am. Chem. Soc.* **2003,** *125*, 6848–6849.

82 J. H. Lim, D. S. Ginger, K. B. Lee, J. Heo, J. M. Nam, C. A. Mirkin, *Angew. Chem. Int. Ed. Engl.* **2003,** *42*, 2309–2312.

83 L. M. Demers, D. S. Ginger, S. J. Park, Z. Li, S. W. Chung, C. A. Mirkin, *Science* **2002,** *296*, 1836–1838.

84 S. Sekula, J. Fuchs, S. Weg-Remers, P. Nagel, S. Schuppler, J. Fragala, N. Theilacker, M. Franueb, C. Wingren, P. Ellmark, C. A. K. Borrebaeck, C. A. Mirkin, H. Fuchs, S. Lenhert, *Small* **2008,** *4*, 1785–1793.

85 J. M. Curran, R. Stokes, E. Irvine, D. Graham, N. A. Amro, R. G. Sanedrin, H. Jamil, J. A. Hunt, *Lab Chip* **2010,** *10*, 1662–1670.

86 S. M. Yang, S. G. Jang, D. G. Choi, S. Kim, H. K. Yu, *Small* **2006,** *2*, 458–475.

87 M. A. Wood, *J. R. Soc. Interface* **2007,** *4*, 1–17.

88 J. R. Jeong, S. Kim, S. H. Kim, J. A. C. Bland, S. C. Shin, S. M. Yang, *Small* **2007,** *3*, 1529–1533.

89 J. Malmstrom, B. Christensen, H. P. Jakobsen, J. Lovmand, R. Foldbjerg, E. S. SÃ¡rensen, D. S. Sutherland, *Nano Lett.* **2010,** *10*, 686–694.

90 N. Walter, C. Selhuber, H. Kessler, J. P. Spatz, *Nano Lett.* **2006,** *6*, 398–402.

91 M. J. Dalby, R. O. C. Oreffo, In Stem Cell Engineering: Principles and Applications; Springer: New York, **2011;** pp 247–258.

92 H. Andersson, A. van den Berg, *Lab Chip* **2004,** *4*, 98–103.

93 T. H. Park, M. L. Shuler, *Biotechnol. Prog.* **2003,** *19*, 243–253.

94 S. H. Lee, A. J. Heinz, S. Shin, Y. G. Jung, S. E. Choi, W. Park, J. H. Roe, S. Kwon, *Anal. Chem.* **2010,** *82*, 2900–2906.

95 G. A. Hudalla, W. L. Murphy, *Soft Matter* **2011,** *7*, 9561–9571.

96 J. T. Koepsel, W. L. Murphy, *Langmuir* **2009,** *25*, 12825–12834.

97 A. G. Mikos, S. W. Herring, P. Ochareon, J. Elisseeff, H. H. Lu, R. Kandel, F. J. Schoen, M. Toner, D. Mooney, A. Atala, M. E. Van Dyke, D. Kaplan, G. Vunjak-Novakovic, *Tissue Eng.* **2006,** *12*, 3307–3339.

98 C. A. Toro, L. A. Arias, S. Brauchi, *Curr. Pharm. Biotechnol.* **2011,** *12*, 12–23.

99 T. M. Keenan, A. Folch, *Lab Chip* **2008,** *8*, 34–57.

100 K. Rajan, In Annual Review of Materials Research; Annual Reviews, **2008**; Vol. *38*, pp 299–322.

101 J. Genzer, R. R. Bhat, *Langmuir* **2008,** *24*, 2294–2317.

102 D. Geblinger, C. Zink, N. D. Spencer, L. Addadi, B. Geiger, *J. R. Soc. Interface* **2012,** *9*, 1599–1608.

103 J. L. Zhang, L. J. Xue, Y. C. Han, *Langmuir* **2005,** *21*, 5667–5671.

104 S. L. Zhang, B. You, G. X. Gu, L. M. Wu, *Polymer* **2009,** *50*, 6235–6244.

105 A. Lagunas, J. Comelles, E. Martinez, J. Samitier, *Langmuir* **2010,** *26*, 14154–14161.

106 J. Genzer, In Annual Review of Materials Research; Annual Reviews, **2012**; Vol. *42*, pp 435–468.

107 B. P. Harris, J. K. Kutty, E. W. Fritz, C. K. Webb, K. J. L. Burg, A. T. Metters, *Langmuir* **2006,** *22*, 4467–4471.

108 N. M. Moore, N. J. Lin, N. D. Gallant, M. L. Becker, *Biomaterials* **2010,** *31*, 1604–1611.

109 Y. Elkasabi, J. Lahann, *Macromol. Rapid Commun.* **2009,** *30*, 57–63.

110 Y. M. Elkasabi, J. Lahann, P. H. Krebsbach, *Biomaterials* **2011,** *32*, 1809–1815.

111 H. Yamazoe, T. Tanabe, *J. Biomed. Mater. Res. Part A* **2009,** *91A*, 1202–1209.

112 N. L. Jeon, H. Baskaran, S. K. W. Dertinger, G. M. Whitesides, L. Van de Water, M. Toner, *Nat. Biotechnol.* **2002,** *20*, 826–830.

113 L. J. Millet, M. E. Stewart, R. G. Nuzzo, M. U. Gillette, *Lab Chip 10*, 1525–1535.

114 J. B. Gurdon, P. Y. Bourillot, *Nature* **2001,** *413*, 797–803.

115 S. K. W. Dertinger, X. Y. Jiang, Z. Y. Li, V. N. Murthy, G. M. Whitesides, *Proc. Natl. Acad. Sci. USA* **2002,** *99*, 12542–12547.

116 B. Li, Y. X. Ma, S. Wang, P. M. Moran, *Biomaterials* **2005,** *26*, 1487–1495.

117 B. M. Lamb, D. G. Barrett, N. P. Westeott, M. N. Yousaf, *Langmuir* **2008,** *24*, 8885–8889.

118 A. Mahapatro, D. M. Johnson, D. N. Patel, M. D. Feldman, A. A. Ayon, C. M. Agrawal, *Nanomed. Nanotechnol. Biol. Med.* **2006,** *2*, 182–190.

119 J. A. Jones, L. A. Qin, H. Meyerson, I. K. Kwon, T. Matsuda, J. M. Anderson, *J. Biomed. Mater. Res. Part A* **2008,** *86A*, 261–268.

120 H. Kondoh, C. Kodama, H. Sumida, H. Nozoye, *J. Chem. Phys.* **1999,** *111*, 1175–1184.

121 J. Noh, M. Hara, *Langmuir* **2001,** *17*, 7280–7285.

122 M. H. Schoenfisch, J. E. Pemberton, *J. Am. Chem. Soc.* **1998,** *120*, 4502–4513.

123 M. Zelzer, M. R. Alexander, N. A. Russell, *Acta Biomater.* **2011,** *7*, 4120–4130.

124 M. R. Alexander, J. D. Whittle, D. Barton, R. D. Short,. *Mater. Chem.* **2004,** *14*, 408–412.

125 M. Notara, N. A. Bullett, P. Deshpande, D. B. Haddow, S. MacNeil, J. T. Daniels, *J. Mater. Sci. Mater. Med.* **2007,** *18*, 329–338.

126 D. B. Haddow, D. A. Steele, R. D. Short, R. A. Dawson, S. MacNeil, *J. Biomed. Mater. Res. Part A* **2003,** *64A*, 80–87.

127 M. T. van Os, Plasma polymers are formed from a glow discharge excited in an organic precursor gas/vapour allowed to flow at a controlled rate into a reaction chamber under reduced pressure. University of Twente, Netherlands, **2000.**

128 F. J. Harding, L. R. Clements, R. D. Short, H. Thissen, N. H. Voelcker, *Acta Biomater.* **2012,** *8*, 1739–1748.

129 H. E. Colley, G. Mishra, A. M. Scutt, S. L. McArthur, *Plasma Process. Polym.* **2009,** *6*, 831–839.

130 V. Sciarratta, K. Sohn, A. Burger-Kentischer, H. Brunner, C. Oehr, *Plasma Process. Polym.* **2006,** *3*, 532–539.

131 M. Zelzer, R. Majani, J. W. Bradley, F. Rose, M. C. Davies, M. R. Alexander, *Biomaterials* **2008,** *29*, 172–184.

132 Y. W. Chun, D. Khang, K. M. Haberstroh, T. J. Webster, *Nanotechnology* **2009,** *20*, 085104.

133 A. Dolatshahi-Pirouz, T. Jensen, D. C. Kraft, M. Foss, P. Kingshott, J. L. Hansen, A. N. *ACS Nano* **2010,** *4*, 2874–2882.

134 I. Wall, N. Donos, K. Carlqvist, F. Jones, P. Brett, *Bone* **2009,** *45*, 17–26.

135 M. Plecko, C. Sievert, D. Andermatt, R. Frigg, P. Kronen, K. Klein, S. Stubinger, K. Nuss, A. Burki, S. Ferguson, U. Stoeckle, B. von Rechenberg, *BMC Musculoskelet. Disord.* **2012,** *13*, 32.

136 K. Mustafa, A. Wennerberg, J. Wroblewski, K. Hultenby, B. S. Lopez, K. Arvidson, *Clin. Oral Implants Res.* **2001,** *12*, 515–525.

137 R. R. Bhat, J. Genzer, B. N. Chaney, H. W. Sugg, A. Liebmann-Vinson, *Nanotechnology* **2003,** *14*, 1145–1152.

138 R. R. Bhat, D. A. Fischer, J. Genzer, *Langmuir* **2002,** *18*, 5640–5643.

139 R. Venkatasubramanian, K. J. Jin, N. S. Pesika, *Langmuir* **2011,** *27*, 3261–3265.

140 Blondiaux, N. Gradients of nanotopography in polymers Dissertation, ETH Zurich, **2006.**

141 J. C. Meredith, J. L. Sormana, B. G. Keselowsky, A. J. Garcia, A. Tona, A. Karim, E. J. *J. Biomed. Mater. Res. Part A* **2003,** *66A*, 483–490.

142 X. Y. Lu, J. L. Zhang, C. C. Zhang, Y. C. Han, *Macromol. Rapid Commun.* **2005,** *26*, 637–642.

143 T. P. Kunzler, C. Huwiler, T. Drobek, J. Voeroes, N. D. Spencer, *Biomaterials* **2007,** *28*, 5000–5006.

144 N. R. Washburn, K. M. Yamada, C. G. Simon, S. B. Kennedy, E. J. Amis, *Biomaterials* **2004,** *25*, 1215–1224.

145 A. Curtis, *IEEE Trans. Nanobiosci.* **2004,** *3*, 293–295.

146 A. M. Ross, Z. X. Jiang, M. Bastmeyer, J. Lahann, *Small* **2012,** *8*, 336–355.

147 C. Zink, H. Hall, D. M. Brunette, N. D. Spencer, *Biomaterials* **2012,** *33*, 8055–8061.

148 Z. B. Liu, L. D. Xiao, B. J. Xu, Y. Zhang, A. F. T. Mak, Y. Li, W. Y. Man, M. Yang, Covalently immobilized biomolecule gradient on hydrogel surface using a gradient generating microfluidic device for a quantitative mesenchymal stem cell study. *Biomicrofluidics* **2012,** *6*, 24111–2411112.

149 V. V. Abhyankar, M. A. Lokuta, A. Huttenlocher, D. J. Beebe, *Lab Chip* **2006,** *6*, 389–393.

150 I. Barkefors, S. Thorslund, F. Nikolajeff, J. Kreuger, *Lab Chip* **2009,** *9*, 529–535.

151 M. V. Turturro, G. Papavasiliou, *J. Biomater. Sci. Polym. Ed.* **2012,** *23*, 917–939.

152 T. A. Kapur, M. S. Shoichet, *J. Biomed. Mater. Res. Part A* **2004,** *68A*, 235–243.

153 D. Guarnieri, De A. Capua, M. Ventre, A. Borzacchiello, C. Pedone, D. Marasco, M. Ruvo, P. A. Netti, *Acta Biomater.* **2010,** *6*, 2532–2539.

154 S. A. DeLong, J. J. Moon, J. L. West, *Biomaterials* **2005,** *26*, 3227–3234.

155 J. K. He, Y. A. Du, J. L. Villa-Uribe, C. M. Hwang, D. C. Li, A. Khademhosseini, *Adv. Funct. Mater.* **2010,** *20*, 131–137.

156 D. E. Discher, P. Janmey, Y. L. Wang, *Science* **2005,** *310*, 1139–1143.

157 L. A. Flanagan, Y. E. Ju, B. Marg, M. Osterfield, P. A. Janmey, *Neuroreport* **2002,** *13*, 2411–2415.

158 Lee-C. Thedieck, N. Rauch, R. Fiammengo, G. Klein, J. P. Spatz, *J. Cell Sci.* **2012,** *125*, 3765–3775.

159 J. R. Tse, A. J. Engler, *PLoS One* **2011,** *6*, 9.

160 T. Luhmann, P. Hanseler, B. Grant, H. Hall, *Biomaterials* **2009,** *30*, 4503–4512.

161 M. C. Dodla, R. V. Bellamkonda, *Biomaterials* **2008,** *29*, 33–46.

162 A. P. Wong, Perez-R. Castillejos, J. C. Love, G. M. Whitesides, *Biomaterials* **2008,** *29*, 1853–1861.

163 M. C. Dodla, R. V. Bellamkonda, *J. Biomed. Mater. Res. Part A* **2006,** *78A*, 213–221.

164 X. Q. Wang, E. Wenk, X. H. Zhang, L. Meinel, Vunjak-G. Novakovic, D. L. Kaplan, *J. Controlled Release* **2009,** *134*, 81–90.